Composition and sources of carbonaceous aerosol in the European Arctic at Zeppelin Observatory, Svalbard (2017 to 2020)

Karl Espen Yttri[1*], Are Bäcklund[1], Franz Conen[2], Sabine Eckhardt[1], Nikolaos Evangeliou[1], Markus Fiebig[1], Anne Kasper-Giebl[3], Avram Gold[4], Hans Gundersen[1], Cathrine Lund Myhre[1], Stephen Matthew Platt[1], David Simpson[5,6], Jason D. Surratt[4,7], Sönke Szidat[8], Martin Rauber[8], Kjetil Tørseth[1], Martin Album Ytre-Eide[1], Zhenfa Zhang[4] and Wenche Aas[1]

[a]The Climate and Environmental Research Institute NILU, Kjeller, Norway.

[2]Department of Environmental Sciences, University of Basel, Basel, Switzerland

[3]TU Wien, Insitute of Chemical Technologies and Analytics, 1060 Vienna, Austria

[4]Department of Environmental Sciences and Engineering, Gillings School of Global Public Health, University of North Carolina at Chapel Hill, Chapel Hill, NC 27599, USA

[5]EMEP MSC-W, Norwegian Meteorological Institute, Oslo, Norway

[6]Department of Earth & Space Sciences, Chalmers Univ. Technology, Gothenburg, Sweden

[7]Department of Chemistry, College of Arts and Sciences, University of North Carolina at Chapel Hill, Chapel Hill, NC 27599, USA

[8]Department of Chemistry, Biochemistry and Pharmaceutical Sciences & Oeschger Centre for Climate Change Research, University of Bern, 3012 Bern, Switzerland

*To whom correspondence should be addressed: E-mail address: key@nilu.no

Abstract

We analyzed long-term measurements of organic carbon, elemental carbon, and source-specific organic tracers from 2017 to 2020 to constrain carbonaceous aerosol sources in the rapidly changing Arctic. Additionally, we used absorption photometer (Aethalometer) measurements to constrain equivalent BC from biomass burning (eBC_{BB}) and fossil fuel combustion (eBC_{FF}), using Positive Matrix Factorization (PMF).

Our analysis shows that organic tracers are essential in understanding Arctic carbonaceous aerosol sources. Throughout 2017 to 2020, levoglucosan exhibited bimodal seasonality, reflecting emissions from residential wood combustion (RWC) in the heating season (November to May) and from wildfires (WF) in the non-heating season (June to October), demonstrating a pronounced inter-annual variability in the influence of WF. Biogenic secondary organic aerosol (BSOA) species (2-methyltetrols) from isoprene oxidation was only present in the non-heating season, peaking in July to August. Warm air masses from Siberia led to a substantial increase in 2-methyltetrols in 2019 and 2020 compared to 2017 to 2018. This highlights the need to investigate the contribution of local sources vs. long-range atmospheric transport (LRT), considering the temperature sensitivity of biogenic volatile organic compounds emissions from Arctic vegetation. Tracers of primary biological aerosol particles (PBAP), including various sugars and sugar-alcohols, showed elevated levels in the non-heating season, albeit with different seasonal trends, whereas cellulose had no apparent seasonality. Most PBAP tracers and 2-methyltetrols peaked during influence of WF emissions, highlighting the importance of measuring a range of source specific tracers to understand sources and dynamics of carbonaceous aerosol. The seasonality of carbonaceous aerosol was strongly influenced by LRT episodes, as background levels are extremely low. In the non-heating season, the organic aerosol peak was as influenced by LRT as was elemental carbon during the Arctic Haze period.

Source apportionment of carbonaceous aerosol by Latin Hypercube Sampling showed mixed contributions from RWC (46%), fossil fuel (FF) sources (27%), and BSOA (25%) in the heating season. In contrast, the non-heating season was dominated by BSOA (56%), with lower contributions from WF (26%) and fossil fuel sources (15%).

Source apportionment of eBC by PMF showed that fossil fuel combustion dominated eBC (70 ± 2.7%), whereas RWC (22 ± 2.7%) was more abundant than WF (8.0 ± 2.9%). Modeled BC concentrations from FLEXPART attributed an almost equal share to fossil fuel sources (51 ± 3.1%) and to biomass burning. Both FLEXPART and the PMF analysis concluded that RWC is a more important source of (e)BC than WF. However, with a modeled RWC contribution of 30 ± 4.1% and WF of 19 ± 2.8%, FLEXPART suggests relatively higher contributions to eBC from these sources. Notably, the BB fraction of EC was twice as high as that of eBC, reflecting methodological differences between source apportionment by LHS and PMF. However, important conclusions drawn are unaffected, as both methods indicate the presence of RWC- and WF-sourced BC at Zeppelin, with a higher relative BB contribution during the non-heating season.

In summary, organic aerosol (281 ± 106 ng m^{-3}) constitute a significant fraction of Arctic PM_{10}, although surpassed by sea salt aerosol (682 ± 46.9 ng m^{-3}), mineral dust (613 ± 368 ng m^{-3}) and typically non-sea-salt sulfate SO_4^{2-} (314 ± 62.6 ng m^{-3}), originating mainly from anthropogenic sources in winter and from natural sources in summer.

1 Introduction

The arctic is warming significantly faster than the rest of the planet due to Arctic amplification (Serreze and Barry, 2011; Schmale et al., 2021). These rapid changes affect atmospheric transport and removal of Arctic aerosols (Jiao and Flanner, 2016), aerosol relative source contributions (Heslin-Rees et al., 2020), vegetation and the carbon cycle (Kramshoj et al., 2016).

Long-range atmospheric transport (LRT) of air masses from lower latitudes is an important driver of the Arctic aerosol burden since local emissions are relatively much lower (e.g., Quinn et al., 2007). However, the importance of LRT may be decreasing since low latitude anthropogenic aerosol emissions are declining (Coen et al., 2020), while high latitude sources are increasing in importance. These include, for example, increased wildfires (WF) (McCarty et al., 2021), sea salt aerosol (SSA) (Heslin-Rees et al., 2020), aeolian mineral dust (MD) following glacial retreat (Zwaaftink et al., 2016), primary biological aerosol particles (PBAP) due to thawing permafrost and Arctic greening (Myers-Smith et al., 2020), which is also likely increasing biogenic volatile organic compounds emission rates and hence biogenic secondary organic aerosol (BSOA) (Hallquist et al., 2009). These changes in sources are also changing Arctic aerosol physical-chemical properties and hence their climate impact. Some PBAP are efficient ice nucleating particles at high temperatures (Tobo et al., 2019), while BSOA might act as cloud condensation nuclei or influence their activity (Riipinen et al., 2011), and have negative feedback to the Arctic climate (Paasonen et al., 2013). Knowledge regarding concentration, activation temperature, composition, sources, origin, and seasonality of Arctic ice nucleating particles and cloud condensation nuclei has a noticeable focus given its relevance to the Arctic climate (Creamean et al., 2018; 2019; 2020; 2022 Hartmann et al., 2019; 2020; Freitas et al., 2023). The aerosol indirect effect is particularly important in the Arctic, as mixed phase clouds have a long lifetime, possibly due to a lack of ice nucleating particles (Solomon et al., 2018), thus changes ice nucleating particles are deemed more important than cloud condensation nuclei regarding Arctic cloud radiative properties (Solomon et al., 2018).

Understanding changes in local aerosol emissions and formation, shifts in LRT of aerosols, and consequently, alterations in the aerosol chemical composition are essential for understanding the evolving Arctic environment and its regional and global climate impacts. Confirming and understanding these changes in atmospheric composition requires high-quality, long-term observations. This is particularly true for carbonaceous aerosol (CA), except for black carbon (BC), a focus of attention due to its impact on climate and albedo (Clarke and Noone, 1985; Pueschel and Kinne, 1995; Hansen and Nazarenko, 2004; Elefteriadis et al., 2009; Hirdmann et al., 2010). A second exception is methane

sulfonic acid (MSA) with time series from 1977 at Alert (Sharma et al., 2019) and 1980 at Barrow (Quinn et al., 2009), though its role in aerosol formation, growth, and radiative forcing is still a matter of ongoing research (Hodshire et al., 2019).

Significant contributions to Organic matter (OM) of Eurasian origin to Arctic Haze (AH) have been suggested since the 1970s (Quinn et al., 2007), quantified mostly as a residual fraction (Quinn et al., 2002) or from measurements of selected organic species (Li et al., 1993). Even short-term, direct, measurements of organic carbon (OC) or OM are scarce (e.g., Hansen et al., 2014; Barrett et al., 2015; Ferrero et al., 2019), limiting our understanding of even basic parameters such as seasonality, annual mean, or inter annual variability. The nearly two-year long study of Ricard et al. (2002) at Sevettjärvi (Finland) is one of three exceptions, though at a latitude of < 70° N, and hence not representative of the high Arctic, with e.g., lower AH and more biogenic volatile organic compounds in summer. Barret et al. (2017) report 1 year of OC data at Barrow, whereas Moschos et al. (2022) presented the most comprehensive study on Arctic OA to this date with up to 3 years of data from 8 Artic sites.

OC levels are not useful in elucidating sources per se, and supporting information is generally needed. For example, elemental carbon (EC) (or equivalent black carbon, eBC) demonstrates the presence of OC from fossil fuel (FF) combustion and biomass burning (BB), essential to source apportionment efforts and monitoring of the otherwise unperturbed Arctic atmosphere. Winiger et al. (2019), attributed 25 ± 16% of EC to BB in winter and 42 ± 19% in summer by radiocarbon (^{14}C) analysis in their Pan-Arctic study. Further separation of BB into residential wood combustion (RWC), WF and agricultural waste burning (AWB) requires inclusion of satellite observations such as MODIS (Moderate Resolution Imaging Spectroradiometer) (Giglio et al., 2003), and transport modelling (Stohl et al., 2006), although seasonality can be a useful qualifier. Stohl et al. (2013) pointed to gas and oil industry flaring as a major source, contributing 42% to Arctic annual mean BC surface concentrations. ^{14}C analysis by Barrett et al. (2017) shows that contemporary OC from biogenic emissions dominated in summer, while contemporary and fossil OC levels were approximately equally large in winter. Moschos et al. (2022) used positive matrix factorization (PMF) on spectral data derived from water-soluble organic carbon extracts, analyzed off-line using an aerosol mass spectrometer. Their study identified three factors dominated by anthropogenic sources (Oxygenated Organic Aerosol, Arctic Haze, and Primary Organic Aerosol) and three factors associated with natural emissions (Methane Sulfonic Acid-Related Organic Aerosol, Primary Biological Organic Aerosol, and Biogenic Secondary Organic Aerosol). These factors exhibited distinct seasonal patterns, with the first three dominating in winter and the latter three in summer.

Source specific organic tracers identified in the Arctic include levoglucosan, mannosan and galactosan (e.g., Schneidemesser et al., 2009; Fu et al., 2013; Zangrando et al., 2013; Hu et al., 2013a; Yttri et al., 2014; Feltracco et al., 2020), which are combustion products of cellulose and hemi-cellulose serving to trace biomass burning emissions (Simoneit et al., 1999). Sugars, sugar-alcohols (here: glucose, fructose, trehalose, arabitol, and mannitol) and cellulose are used for tracing PBAP (Graham et

al., 2003; Elbert et al., 2007; Sanchez-Ochoa et al., 2007), with sugar-alcohols typically associated with yeast and fungal spores, and sugars linked to pollen, fern spores and other giant bioaerosol (Graham et al., 2003). Cellulose, a primary component of plant cell walls, is used to trace plant debris (Sanchez-Ochoa et al., 2007). Sugars and sugar-alcohols have previously been detected in Arctic aerosol (e.g., Fu et al., 2009b; Fu et al., 2013; Feltracco et al., 2020), but cellulose has not been reported in these studies. Oxidation products of isoprene (e.g., 2-methyltetrols), monoterpenes (e.g., 3-Methyl-1,2,3-butane-tricarboxylic acid), and sesquiterpenes (e.g., β-caryophyllinic acid) are all BSOA species previously detected in the Arctic aerosol (Fu et al., 2009a; Fu et al., 2013; Hansen et al., 2014; Hu et al., 2013). Most studies measuring organic tracers in the Arctic have been limited to short time periods or specific seasons, lacking a comprehensive understanding of the seasonal, annual and interannual variability of sources and their impact on Arctic CA. Notable exceptions are the one-year study of Hansen et al. (2014) and Yttri et al. (2014), along with the multi-seasonal investigation of Feltracco et al. (2020).

Lack of long-term OA measurements limits knowledge of Arctic aerosol mass closure. Further, OA speciation, needed for source attribution and for studying its impact on cloud condensation nuclei and ice nucleating particles is scarce. Here, we present four years of OC and EC, organic tracer, and eBC_{BB} and eBC_{FF} measurements made at the high Arctic Zeppelin Observatory (Ny-Ålesund, Svalbard), providing multiyear insights to Arctic CA and the fundamental knowledge needed to understand changes in Arctic cloud condensation nuclei and ice nucleating particles and hence the impact of a changing Arctic on regional and global climate.

2 Experimental

2.1 Sampling site

The Zeppelin Observatory (78°5' N 11°5' E, 472 m above sea level, asl) is located on the Zeppelin Mountain on the 20 km long and 10 km wide Brøgger peninsula, 2 km south of the remote Ny-Ålesund settlement on the west coast of the Spitsbergen Island in the Svalbard archipelago (Norway, Fig. 1; Platt et al., 2022). The 26 km long Kongsfjorden to the northeast and the 88 km long Forland straight in the west, surround the peninsula. The Observatory lies in the northern Arctic tundra zone, surrounded by barren ground largely consisting of bare stones, and occasionally a thin layer of topsoil with scarce ground vegetation, mostly growing on plains at lower altitudes, and snowpacks, and glaciers. There is very little influence of emissions from the Ny-Ålesund settlement, as the Observatory is typically above the boundary layer.

The Svalbard climate reflects its high Northern latitude, but is moderated by the North Atlantic Current, with substantially higher temperatures than at corresponding latitudes in continental Russia and Canada, particularly in winter. Hence, the Kongsfjorden basin is considered relatively verdant due to its favorable micro-climate, and ~180 plant species, 380 mosses, and 600 lichens are registered on the Svalbard Archipelago (Vegetation in Svalbard, 2023). However, a short growing season (June to August), 4 months of polar night, and 8 to 9 months of snow (Fig. 2) do not provide optimal conditions

for growth (Karlsen et al., 2014). Annual precipitation in Western Svalbard is around 400 mm.

The Zeppelin Observatory is part of many networks including the European Evaluation and Monitoring Program (EMEP, www.emep.int), the Global Atmospheric Watch (GAW, https://public.wmo.int/en/programmes), the Arctic Monitoring and Assessment Program (AMAP, www.amap.no), and is included in the EU infrastructure ACTRIS (Aerosols, Clouds and Trace gases Research InfraStructure Network, www.actris.eu)

2.2 Sampling, handling, and storage of ambient aerosol filter samples

We used a Digitel high-volume sampler (PM_{10} inlet, flow rate 666 L min^{-1}, filter face velocity 72.1 cm s^{-1}) to obtain ambient aerosol filter samples. We placed the sampling inlet 2 m above the Observatory roof and 7 m above ground level. We collected aerosol particles on pre-fired (850 °C; 3 h) quartz fiber filters (PALLFLEX Tissuequartz 2500QAT-UP; 150 mm in diameter) at a weekly time resolution. There was some variability in sampling time, typically due to harsh weather conditions. We used a quartz fiber filter behind quartz fiber filter (QBQ) set up to estimate the positive sampling artifact of OC (McDow and Huntzicker, 1990). We shipped the filters in their respective filter holders, wrapped in baked aluminum foil, and placed them in double zip lock bags. Before exposure and analysis, we stored the samples in a freezer (-18°C). For each 1.5 month of sampling, we assigned one field blank, which was treated in the same manner regarding preparation, handling, transport, and storage as the exposed filters, except that they were not inserted in the sampler.

We collected the aerosol filter samples from 5 January 2017 to 4 January 2021 as part of the Norwegian national monitoring programme (Aas et al., 2020)

2.3 Measurement of OC and EC

We performed Thermal-optical analysis (TOA) using the Sunset Lab OC/EC Aerosol Analyzer. We used transmission for charring correction and operated the instrument according to the EUSAAR-2 temperature program (Cavalli et al., 2010). As part of the joint EMEP/ACTRIS quality assurance and quality control effort, we regularly intercompared the performance of the OC/EC instrument (e.g., Cavalli et al., 2016).

2.4 Measurement of organic tracers

2.4.1 Monosaccharide anhydrides, 2-methyltetrols, sugars, and sugar-alcohols

We determined concentrations of monosaccharide anhydrides, sugar-alcohols, 2-methyltetrols, monomeric and dimeric sugars in PM_{10} filter samples using ultra-performance liquid chromatography (UPLC) (Vanquish UPLC, Thermo) in combination with Orbitrap Q-Exactive Plus (Thermo Fischer Scientific) operated in the negative electrospray ionization (ESI) mode: resolution 70 000 FWHM (full width at half maximum) at 200 Dalton.

We added isotopically labelled internal standard to filter punches (2 × 1.5 cm^2), which were

submerged in precleaned tetrahydrofuran (THF) (2 mL) in separate screw neck amber glass vials, which we subjected to ultrasonic extraction (30 min). We transferred the solute to a centrifuge tube using pipetting and repeated this step twice. Afterward, we evaporated the solute to 0.4 mL, spun it (10 min; 2000 rpm), transferred and evaporated it to dryness in a screw neck amber glass vial. The sample volume was redissolved in 0.25 mL precleaned THF/Milli-Q water (55:45) and whirlmixed before analysis. The extraction procedure was equal to Dye and Yttri (2005). We used two columns in series for separation (two 3.0 mm × 150 mm HSS T3, 1.8 µm, Waters Inc.), using isocratic elution (Milli-Q; 18.2 MΩ), flushing with acetonitrile (High purity) at the end of the run. The Milli-Q water was purified using and EDS-Pak Polisher, containing activated coal (Merck, Darmstadt, Germany), and a LC-Pak cartridge (Merck, Darmstadt, Germany) containing reversed-phase silica.

We identified all species based on retention time and mass spectra of authentic standards, using isotope-labelled standards of levoglucosan, galactosan, mannitol, arabitol, trehalose and glucose as recovery standards (Table S1 in Yttri et al., 2021). The limit of detection (LOD) was 1 to 3 pg m^{-3} for the monosaccharide anhydrides, 1 pg m^{-3} for the 2-methyltetrols, 4 pg m^{-3} for the sugar-alcohols, 6 pg m^{-3} for the dimeric sugars and 8 pg m^{-3} for the monomeric sugars.

2.4.2 Measurement of cellulose

We based the analysis of free cellulose on the saccharification of cellulose and subsequently quantified the glucose produced, following the method by Kunit and Puxbaum (1996). We switched the final detection of glucose from a photometric method to HPAEC PAD (high-performance anion-exchange chromatography with pulsed amperometric detection), similar to Qi et al., 2020). We extracted filter aliquots with a citrate buffer (0.05 M citric acid) adjusted to pH 4 and added Thymol to a final concentration of 0.05% to prevent bacterial growth. We enhanced extraction by ultrasonic agitation. We added enzymes (Trichoderma reesei cellulase; Aspergillus Niger cellobiase), which had been precleaned by ultrafiltration to reduce glucose blanks, for saccharification. We stopped saccharification (at 45 °C) after 24 h by heating the samples to 80 °C. We analyzed glucose on a Dionex ICS 3000 equipped with a CarboPac MA1 column, using a sodium hydroxide gradient reaching from 480 mM NaOH to 630 mM. We corrected results with the free glucose contained in the samples.

2.5 Radiocarbon measurements

We conducted ^{14}C-measurements of TC and EC by complete combustion of the untreated quartz fiber filter and after removal of OC, respectively, using thermal-optical analysis (760 °C, pure O_2) coupled with on-line measurement in an accelerator mass spectrometer (Agrios et al., 2015). For a detailed description of the analytical method and data processing, see Rauber et al. (2023).

2.5.1 Selection criteria for samples subject to radiocarbon analysis

We picked 1 – 2 filter samples for each month of the year from samples collected from 2017 to 2018 to

capture the seasonal variability in source composition (Table S3). No valid solution was found for the sample 05 – 13.12.2017, using the Latin Hypercube Sampling (LHS) approach (Sect. 2.8), hence the low coverage for December (6%) compared to September (77%). We pooled two consecutive samples for the months of June, July, August, September, October, and December to meet the LOD (3 µg C) for EC. Moreover, we aimed for the front/back filter carbon content ratio >3, but this criterion was not met for one of the samples in June, September, October, and for two samples in December.

We analyzed ^{14}C-TC on both front and back filters, while ^{14}C-EC was analyzed only on front filters. To measure ^{14}C-EC, we used three circular punches (22 mm diameter) from the filter sample aliquot (16.6 cm^2). We used the remaining front filter area (5.2 cm^2) for ^{14}C-TC analysis, along with an equivalent area of the back filter.

2.6 Measurement of the aerosol absorption coefficient by multi wavelength Aethalometer

We obtained measurements of aerosol absorption coefficient (Babs) using a 7-wavelength (370, 470, 520, 590, 660, 880, and 950 nm) absorption photometer (AE33 Aethalometer, Magee Scientific) downstream of a PM_{10} inlet, yielding equivalent black carbon (eBC) by normalization with co-located EC measurements. We determined two eBC categories using a novel application of positive matrix factorization (PMF) (Yttri et al., 2021; Platt et al., in prep.). These categories were based on the Aerosol Ångstrøm Exponent (AAE), with one having a low AAE (~1), resulting from efficient combustion of mainly liquid fossil fuel, denoted eBC_{FF}, and the other having a high AAE (~1.6), mainly associated with biomass burning (eBC_{BB}) and possibly residential coal combustion.

2.7 Auxiliary data

We downloaded concentrations of SO_4^{2-}, Cl^-, Na^+, K^+, Mg^{2+}, Ca^{2+}, Al, Fe, Mn, and Ti from the EBAS data repository (https://ebas-data.nilu.no). Inorganic anions and cations were obtained using a NILU stacked filter unit (SFU) collecting aerosol particles on Teflon filters (2 µm pore, 47 mm Zefluor Teflon, Gelman Sciences). The SFU has a downward-facing inlet that effectively reduces the sampling efficiency for aerosol particles with an equivalent aerodynamic diameter (EAD) larger than 10 µm (Zwaaftink et al., 2022). Elements were obtained from paper filters (Whatman 41) using a high-volume air sampler with an inlet discriminating against aerosol particles with an EAD larger than 3 µm.

We calculated sea salt (ss) aerosol (SSA) according to equations 1 – 5, and mineral dust (MD) according to equations 6 and 7. We assumed Al, Fe, Mn, and Ti to be associated exclusively with mineral dust and present as Al_2O_3, Fe_2O_3, MnO, and TiO_2 (Alastuey et al., 2016). Si data was not available and thus estimated based on an empirical factor (eq. 7), assumed present as SiO_2.

$$[SSA] = [Na^+] + [Cl^-] + [ssK^+] + [ssMg^{2+}] + [ssCa^{2+}] + [ssSO_4^{2-}] \quad \text{(eq. 1)}$$

$$[ssK^+] = [Na^+] \times 0.037 \quad \text{(eq. 2)}$$

$$[ssMg^{2+}] = [Na^{+}] \times 0.12 \quad \text{(eq. 3)}$$

$$[ssCa^{2+}] = [Na^{+}] \times 0.038 \quad \text{(eq. 4)}$$

$$[ssSO_4^{2-}] = [Na^{+}] \times 0.252 \quad \text{(eq. 5)}$$

$$[MD] = [SiO_2] + [Al_2O_3] + [Fe_2O_3] + [MnO] + [TiO_2] \quad \text{(eq. 6)}$$

$$[SiO_2] = 2.5 \times [Al_2O_3] \quad \text{(eq. 7)}$$

2.8 Source apportionment of carbonaceous aerosol by Latin Hypercube Sampling

We used a Latin Hypercube Sampling (LHS) approach (Gelenscer et al., 2007; Yttri et al., 2011a) for source apportionment of CA, using ^{14}C, organic tracers, and OC and EC measurements from 13 samples (Table S3) as input. We quantified seven CA fractions: EC from combustion of biomass (EC_{bb}) and fossil fuel (EC_{ff}), OC from combustion of biomass (OC_{bb}) and from fossil fuel sources (OC_{ff}), primary biological aerosol particles (OC_{PBAP}), being the sum of plant debris (OC_{pbc}) and fungal spores (OC_{pbs}), and secondary organic aerosol (SOA) from biogenic precursors (OC_{BSOA}). Our calculations were based on similar equations and emission ratios (ER) to those presented in Yttri et al. (2011a), except that we used ^{14}C-EC to calculate OC_{BB} and EC_{BB}. We have provided updated equations and ERs in Tables S1 to S2. At a remote site like Zeppelin where BB emissions originate from distant source regions, ^{14}C-EC seems a better option for apportioning BB emission than levoglucosan, assuming significant depletion of levoglucosan under such conditions. Calculated concentrations and fractions of the CA categories are presented in Tables S3 and S4. The NH-season was covered by 98 days, while the heating (H) season was covered by 54 days.

2.9 FLEXPART modelling

We calculated BC concentrations at Zeppelin using the Lagrangian particle dispersion model FLEXPART version 10.4 (Pisso et al., 2019). FLEXPART released computational particles every 3 h for the whole study period at the Zeppelin Observatory, which were tracked backward in time. The model was driven by ERA5 (Hersbach et al., 2020) assimilated meteorological analyses from the European Centre for Medium-Range Weather Forecasts (ECMWF) with 137 vertical layers, a horizontal resolution of 0.5° × 0.5°-, and one-hour temporal resolution. We kept the particles in the simulation for 30 days after release, sufficient to include most BC emissions arriving at the site, given a typical BC lifetime of 1 week (Bond et al., 2013). FLEXPART simulates dry and wet deposition of gases or aerosols (Grythe et al., 2017), turbulence (Cassiani et al., 2014), unresolved mesoscale motions (Stohl et al., 2005), and includes a deep convection scheme (Forster et al., 2007). Footprint emission sensitivities were calculated at spatial resolution of 0.5° × 0.5°. We assumed that BC has a density of 1500 kg m^{-3}, following a logarithmic size distribution with an aerodynamic mean diameter of 0.25 µm and a logarithmic standard deviation of 0.3 (Long et al., 2013).

The footprint emission sensitivities express the probability of any release occurring in each grid-cell to reach the receptor site. When coupled with gridded emissions from any emission inventory, it can be converted to modelled concentration at the receptor site. To derive the contribution to receptor BC from different sources, we combined each gridded emission sector (e.g., gas flaring, transportation) with the footprint emission sensitivity. We used anthropogenic emissions from the latest version (v6b) of the ECLIPSE (Evaluating the CLimate and Air Quality ImPacts of ShortlivEd Pollutants) dataset, which is an upgraded version of the previous version 5a, as described by Klimont et al. (2017). The inventory (provided with a spatial resolution of 0.5° × 0.5°, monthly) includes:

- Industrial combustion (IND) – emissions from industrial boilers and industrial production processes
- Energy production (ENE) – combustion processes in power plants and generators.
- Residential and commercial sector (DOM) – combustion in heating, cooking stoves, and boilers in households, public, and commercial buildings.
- Waste treatment and disposal sector (WST) – emissions from waste incineration and treatment.
- Transport sector (TRA) – emissions from all land-based transport of goods, animals, and persons on road and off-road networks, including domestic shipping and aviation.
- Emissions from international shipping activities (SHP).
- Gas flaring (FLR) – emissions from oil and gas facilities.

The ECLIPSEv6b dataset provides emission data at 5-years intervals. These emissions are then interpolated to annual emissions according to the trend in geographical areas considered in ECLIPSE (Klimont et al., 2017). The temporal variation in the emissions of all sectors was provided by IIASA (Klimont et al., 2017). WF emissions were adopted from the Global Fire Emission Dataset version 4.1 (GFEDv4.1). The product combines satellite information on fire activity and vegetation productivity to estimate gridded monthly burned area and fire emissions, as well as scalars that we can use to calculate higher temporal resolution emissions. All data are publicly available for use in large-scale atmospheric and biogeochemical modelling (van der Werf et al., 2017). Emission factors to compute BC emissions are based on Akagi et al., (2011). The spatial resolution of the current version (v4) is of 0.25° × 0.25°, daily.

To distinguish between modelled BC_{bb} and BC_{ff}, we combined contributions to receptor concentrations from (i) DOM and WF, and (ii) ENE, FLR, IND, WST, SHP and TRA, respectively.

3 Results and discussion

Monthly mean concentrations of OC, EC, and organic tracers at Zeppelin Observatory are presented in Fig. 2 and Fig. 3, and annual and seasonal means in Table 1. Our study is the first presenting eBC_{BB} and eBC_{FF} data (Fig. 2) derived from multiwavelength aethalometer measurements in the Arctic, and we

compare them with BC_{BB} and BC_{FF} data obtained from the FLEXPART model (Table 3; Fig. 4; Fig S1) and with EC_{BB} and EC_{FF} data from the LHS-approach (Sect. 3.2.1) (Table 4; Table S3 to S4). CA source apportionment by the LHS-approach is presented in Fig. 5 and Tables S3 to S4. We discuss our data according to the periods June to October, representing the growing season and the non-heating season (NH-season), and November to May covering the non-growing season and the heating season (H-season). These are obviously not absolute definitions. Phenomena of high relevance to the Arctic aerosol, such as Boreal WF emissions thus largely reside in the NH-season, whereas accumulation of anthropogenic emissions from Eurasia in winter and spring, known as AH, is part of the H-season. Comparison is made with Birkenes Observatory (Southern Norway), representative of the lowest CA levels in regional background Europe (Yttri et al., 2021) (Table S5 and S6), with Ispra, a regional background site in the Po Valley (Northern Italy), one of Europe's most polluted regions (Table 5S), and the Trollhaugen Observatory (Antarctica) (S7).

3.1 Elemental carbon and organic carbon

The interannual variabilities of EC (34%) and OC (38%) were comparable to SO_4^{2-} (40%). Like OC, SO_4^{2-} can have both primary or secondary sources, originate from LRT or local emissions, and stem from natural as well as anthropogenic sources. Notably, its time series spans back to 1991 (Platt et al., 2022). The annual mean concentrations ranged from 6.5 to 16.3 ng Carbon (C) m^{-3} for EC and from 90.3 to 197 ng C m^{-3} for OC. These levels are amongst the lowest globally, still notably lower compared to Antarctica (1.9 ng EC m^{-3}; 12.2 ng OC m^{-3}) (Table S7) (Rauber et al., in prep.). Particulate OC (OC_P) had an estimated conservative concentration of 68.3 to 165 ng C m^{-3} after accounting for the positive sampling artifact (OC_B). CA levels were particularly high in 2020 due to a major LRT episode in July (Sect. 3.6.1), with EC and OC increased by factors of 1.6 and 1.9, respectively compared to the mean of the previous three years. For SO_4^{2-}, the increase in 2020 was only 1.25.

The annual mean concentration of OM (281 ± 106 ng m^{-3}) was less than for sea salt aerosol, mineral dust, and even non-sea salt SO_4^{2-}, although not for all four years considered (OM > nss SO_4^{2-} for 2020) (Table 2).

Elevated EC concentration in the H-season correspond with the AH phenomenon (Shaw, 1995), and is consistent to that previously shown for eBC (Eleftheriadis et al., 2009) and SO_4^{2-} (Quinn et al., 2007; Platt et al., 2022). However, three of the four highest weekly EC concentrations occurred in the NH-season (Sect. 3.5). The mean EC concentration in the NH-season was five times lower than at the Birkenes Observatory, and close to two orders of magnitude lower than Ispra. EC increased by a factor of two during the H-season compared to the NH-season, due to more efficient transport of air masses to the Arctic in winter (Ottar et al., 1989) and by AH accumulation in winter and spring (Shaw, 1995). The EC level at Zeppelin in the NH-season was eight times lower than at Birkenes and nearly 60 times lower than at Ispra.

OC levels at Zeppelin was seven times lower than at the Norwegian mainland both for the H-

and NH-seasons. In the H-season, levels at Zeppelin were more than 50 lower than in the polluted Po Valley region, while slightly more than one order of magnitude lower in the NH-season.

OC seasonality (Fig. 2) was characterized by a dip in May and June, a transition period between the elevated levels seen for the AH period and the mid-summer. Contemporaneous measurements of organic tracers (BB, BSOA and PBAP), EC, eBC_{BB} and eBC_{FF}, largely explained the seasonality. EC was elevated throughout the AH period, pointing to a dominant contribution of OC from combustion of FF and BB, whereas BSOA and PBAP tracers (except for cellulose) did not start increasing until June. Note that Fu et al. (2009a) found terpene oxidation products, such as 3-Methyl-1,2,3-butane-tricarboxylicacid (3-MBTCA) to be elevated compared to most isoprene oxidation products during the AH period at Alert (Canadian Arctic), and that only isoprene oxidation products were measured in the present study. Further, results presented in section 3.5 suggest a 25% BSOA contribution to CA even in winter. The BB tracer levoglucosan experienced a significant decrease from February to March, suggesting that OC from fossil sources became more prominent as the AH period progressed. However, we speculate that there was a substantial degradation of levoglucosan starting from the end of the polar night (15 February) or as daylight hours increased, as no similar decrease was observed for eBC_{BB}. This degradation might be due to factors such as aerosol particle scavenging by low-level Arctic clouds, which is known to peak in early spring for BC (Zieger et al., 2023), and subsequent depletion by water phase reactions. BB, BSOA and PBAP tracers typically peaked in July and August, but whereas BSOA tracers decreased abruptly in early fall, PBAP tracers persisted to late fall, whereas BB tracers, EC, eBC_{BB}, and eBC_{FF} started increasing again towards the end of the year.

Eight of the ten highest OC concentrations were observed in the NH-season, while for EC, seven of the ten highest concentrations were observed in the H-season. Low emissions within the Arctic make OC, and EC, seasonality susceptible to LRT episodes, and we find that the OC peak in the NH-season is as strongly influenced by LRT as is EC during AH. We discuss three of these episodes in section 3.5.

3.2 Biomass burning and fossil fuel combustion sources

3.2.1 Levoglucosan

Annual mean levoglucosan concentrations ranged from 0.335 to 0.919 ng m^{-3}, which is comparable to the annual mean (0.680 ng m^{-3}) reported for Zeppelin for March 2008 to March 2009 (Yttri et al., 2014). The inter annual variability was 40%, similar to major aerosol constituents such as OC and SO_4^{2-}. In 2020, the annual mean was twice as high as the mean of the previous three years, with an increase attributed to elevated monthly means (~2 ng m^{-3}) in February, July, and October (Fig. 3).

Increased levels and peak concentrations of levoglucosan in the H-season reflected RWC emissions, as shown by Yttri et al. (2014). Increased levels in July and August were not shown by Yttri et al. (2014), partly due to missing data, although impact from wild and agricultural fires was predicted by modelling. In the present study, increased levels in July and August were a hallmark of the levoglucosan time series, pointing to the importance of WF emissions. FLEXPART model transport of

448 modelled BC emissions also showed a substantial influence of WF emissions for July and August (2017
449 to 2020) (Fig. S1). The levoglucosan concentration in the 2020 NH-season was ~ 3-times higher than
450 the average of the three previous years, demonstrating a pronounced inter annual variability in WF
451 influence at Zeppelin. The levoglucosan to mannosan ratio (L/M) was lower for the NH-season (4.8 ±
452 1.2) compared to the H-season (7.5 ± 1.9) (Fig. 3; Table S6) and might reflect a shift from WF and AWB
453 in the NH-season to RWC in the H-season. Our findings correspond with L/M ratios below 5 in summer
454 at Gruvebadet (Ny-Ålesund) (Feltracco et al., 2020). However, we did not observe the very high L/M
455 ratios, occasionally exceeding 40, that have been attributed to emissions from crops residue burning in
456 Asia during the spring.
457
458 **3.2.2 EC_{BB} and EC_{FF} obtained from radiocarbon measurements and LHS**
459 Tracer based LHS source apportionment found that BB was the primary source of EC in all but one
460 sample (Table S3 and S4). On average, 61 ± 15% of EC was attributed to BB, with this percentage
461 varying by season: 67 ± 5% in the NH-season when EC levels were low and influenced by WF, and 57
462 ± 18% in the H-season when RWC dominated. Our results showed a much higher BB fraction in the H-
463 season than Winiger et al. (2019) for the H-season 2012 to 2013 (36 to 39%), whereas it matched that
464 of the AH period in 2009 (57 ± 21%) (Winiger et al., 2015). The BB fraction in NH-season was slightly
465 higher than the 58 to 62% range for the NH-season in 2013 (Winiger et al., 2019). Notably, differences
466 in sample preparation and in ^{14}C analytical protocol should be considered along with inter annual
467 variability, seeking an explanation to the observed differences.
468 The weekly maximum BB fraction of EC in Feb. 2017 (81%) was somewhat lower than the
469 extremely high (95 to 98%) daily BB fractions during AH at Zeppelin in 2009 (Winiger et al., 2015).
470 Although no conclusive explanation was given to the extreme values reported by Winiger et al. (2015),
471 it cannot be excluded that that BB emissions can dominate for an entire week. eBC_{BB} apportioned by
472 PMF (Sect. 3.2.3), supports nearly exclusive (90%) BB contributions for 24 h (Fig. S2), but not for an
473 entire week (80%) (not shown). Notably, Kongsfjorden has around twenty cabins and a few research
474 stations, and wood is used for heating in these facilities when in use. Hence, emissions from these
475 sources cannot be excluded. The weekly minimum BB fraction for Jan. 2018 (21%) was much lower
476 compared to the lowest percentage reported by Winiger et al. (2015) (39%). FLEXPART footprints for
477 the Feb. 2017 and the Jan. 2018 samples were similar, covering North-West Russia and North-East
478 Greenland (not shown), providing no further insight to their extreme values, and thus "highlights the
479 complexity of BC in the Arctic atmosphere, where the generally low BC levels may be strongly
480 influenced by point sources or occasional combustion practices" (Winiger et al., 2015).
481
482 **3.2.3 eBC from biomass burning and fossil fuel combustion obtained from PMF and**
483 **FLEXPART modeling**
484 The eBC (sum of eBC_{BB}, and eBC_{FF}) and EC time series were similar, with enhanced levels during AH,

a small increase in mid-summer, and a slight increase towards the end of the year. FF was the major fraction of eBC annually (70 ± 2.7%), in the H-season (71 ± 2.7%), and in the NH-season (67 ± 6.7%) (Table 3; Fig. 4).

Previous modelling studies indicate that WF is the primary source of Arctic BC during summers (Stohl et al., 2013; McCarty et al., 2021). ^{14}C-EC measurements support this for Zeppelin, but not for other high Arctic observatories (Table 4; Winiger et al., 2019). In our study, 27% – 42% of eBC was attributed to WF emissions in the NH-season, which is lower than previous findings. Our estimate assumes that all eBC_{BB} in the NH-season comes from WF emissions (eBC_{WF}) and from residential wood combustion emissions (eBC_{RWC}) in the H-season. Neither eBC_{WF}, nor eBC_{RWC} dominated on a monthly basis (Fig. S3), although they came close in October 2017, July 2020, and October 2020, accounting for 46% to 48%. The annual contribution of eBC_{WF} to eBC was estimated to be 5.4% to 12%, while eBC_{RWC} contributed 20 to 26%, highlighting that RWC is a larger source of eBC compared to WF.

FLEXPART predicted an almost equal share of BC from BB and FF annually, whereas BC_{FF} (56 ± 3.6%) dominated in the H-season and BC_{BB} (61 ± 3.3%) in the NH-season (Table 3), similar to results found in Stohl et al. (2013). For a direct comparison, BC_{WF} (and BC_{RWC}) was calculated similarly from FLEXPART BC_{BB} output as eBC_{WF} from eBC_{BB} by PMF, i.e., BC_{WF} equals all BC_{BB} in the NH-season, whereas BC_{RWC} equals all BC_{BB} in the H-season. Comparing this proxy BC_{WF} with the FLEXPART modelled $BC_{WF,}$ provided a ratio of 0.97 to 1.09 for 2017 to 2020, indicating that the BC_{WF} proxy is a sound approximation. With 16 to 22% of BC attributed to WF and 27 to 36% to RWC annually (Fig. 4; Table 3), FLEXPART concludes, in the same way as PMF, that RWC > WF, but suggests higher percentages for WF and RWC fractions.

Neither PMF nor FLEXPART seem to fully reflect the predominant role of BC from WF above 50 °N, which McCarty et al. (2021) suggest are larger than emissions from anthropogenic residential combustion, transportation, and flaring, combined. In 2020, 56% of the BC emissions North of 65 °N were attributed to open biomass burning by McCarty et al. (2021), whereas 12% (PMF) and 22% (FLEXPART) of (e)BC was attributed to WF at Zeppelin for 2020 in the present study. Spatial variability and vertical distribution of the emissions might explain part of the discrepancy, as might mid latitude emissions below 65 °N, being less influenced by WF. Vertically resolved BC concentrations in the Artic in spring and summer based on aircraft measurements show a decrease with increasing altitude (Jurányi et al., 2023), but this remains yet to be confirmed for BC from WF.

For the BB tracer levoglucosan, the fraction observed in the NH-season (36 to 64%), corresponding to the WF fraction, was higher than seen for both eBC_{WF} (17 to 35%) (PMF) and BC_{WF} (32 to 45%) (FLEXPART). However, degradation of levoglucosan during LRT, and lack of representative (e)BC/levoglucosan ERs for a vast number of fuel categories, vegetation types, and not least combustion conditions, implies considerable uncertainty in deriving the RWC/WF (e)BC split using this technique.

Comparing PMF results to the few samples subjected to ^{14}C measurements and source apportionment by tracer based LHS showed that these two approaches were on opposite ends of the scale, with FLEXPART in between (Table 4). Radiocarbon measurements and LHS estimated a BB fraction twice as high as the PMF approach, but all three methods agreed on a higher BB fraction in the NH-season than in the H-season. Notably, BB and FF fractions of eBC derived from PMF were more aligned with those from radiocarbon measurements at Zeppelin in 2012 to 2013 (Winiger et al., 2019) and with fractions derived from levoglucosan measurements at Zeppelin in winter 2008 to 2009 (Yttri et al., 2014). However, inter-annual variability makes such a comparison indicative only. Consideration of methodological differences is essential. Crucial steps of ^{14}C-EC measurements include preventing EC loss during OC removal and avoiding OC mixing with the minor EC fraction, impacting its modern vs. fossil fuel signature. The advancements in the analytical approach used in this study (Rauber et al., 2023) specifically aimed to improve these critical steps. Additionally, eBC derived from Aethalometer measurements provides no information on the age of carbon undergoing combustion but reflects the wavelength dependence of the absorption linked to the combustion condition (Garg et al., 2016.). Consequently, the eBC_{FF} factor obtained by PMF could also contain emissions from combustion of biofuels, observed as modern carbon by ^{14}C-measurements. Conversely, emissions from coal combustion might contribute to the eBC_{BB} factor. Terms like liquid fuel instead of fossil fuel and solid fuel instead of biomass burning could be more appropriate, but we maintain the notation for comparability with ^{14}C-based apportionment and Aethalometer-model studies (Sandradewi et al., 2008). Applying the Aethalometer-model approach with an Ångstrøm exponent pair of (1,2) (Sandradewi et al. 2008) and (0.9,1.68) (Zotter et al., 2017), yields annual eBC_{BB} contributions of 32% and 29%, supporting our more novel PMF approach (27±14%) (Table 4). Further, we note that the Ångstrøm exponents obtained from the PMF (1,1.6) are consistent with the distribution of Ångstrøm exponents observed at various sites across Europe (e.g., Tobler et al., 2021). Despite the differences in the estimated contribution size from biomass vs. fossil fuel sources between ^{14}C-EC measurements and eBC by PMF, important conclusions drawn are unaffected. For instance, both methods indicate the presence of residential wood combustion and wildfire-sourced black carbon at Zeppelin, with a higher relative BB contribution during the non-heating season.

Nearly exclusive (90%) contributions to eBC were seen for both eBC_{BB} and eBC_{FF} for periods of 24 h (Fig. S2, upper left panel). This corresponds with 24 h ^{14}C-EC data from Zeppelin dominated (EC $f_{bb} > 95\%$) by contemporary carbon (Winiger et al., 2015), and ^{14}C-EC data dominated (EC $f_{ff} > 95\%$) by fossil carbon observed at other high Arctic sites (Winiger et al., 2019). Exclusive contributions were most frequent for eBC_{FF} and seen for 1.1% of the dataset compared to 0.1% for eBC_{BB}. Hence, with a few exceptions, eBC_{BB} and eBC_{FF} co-appear.

3.3 Biogenic secondary organic aerosol - 2-methyltetrols

2-methyltetrols (here: sum of 2-methylerythritol and 2-methylthreitol) are primarily formed from the

acid-catalyzed multiphase chemistry of isoprene epoxydiols (IEPOX) (Surratt et al., 2010; Lin et al., 2012; Cui et al., 2018), which are important low-NO_x oxidation products of isoprene (Paulot et al., 2009), the biogenic volatile organic compound (500 Tg C yr^{-1}) emitted in highest amount globally (Williams and Koppmann, 2007), and an important source of BSOA (Hallqquist et al., 2009; Noziere et al., 2015). Their low-level presence in the Arctic has been demonstrated in only a few studies covering a few months (e.g., Fu et al., 2009a). We discuss their level, seasonality, sources, and LRT vs. local formation over four consecutive years.

2-methyltetrol concentrations at Zeppelin were at the lower range of those reported in Europe (Ion et al., 2005; Kourtchev et al., 2005; 2008 a,b), North-America (Cahill et al., 2006; Xia and Hopke; 200; Cui et al., 2018), South-America (Claeys et al., 2010) and Asia (Fu et al., 2010), and consistent with levels observed at Alert in the Canadian Arctic (Fu et al., 2009a). The duration of the elevated 2-methyltetrols concentrations during the peak of the inter annual cycle at Zeppelin appears quite like that at the Birkenes Observatory (Southern Norway) 2300 km further south: with an onset in June and peak concentrations in July and August, the time series at Zeppelin is delayed by half a month compared to Birkenes (Fig. 6 in Yttri et al., 2021), although concentrations drop by mid-October at both sites. The annual mean 2-methyltetrols concentration was 3 times lower at Zeppelin compared to Birkenes in 2017 and 5 in 2018. In 2019, the 2-methyltetrol level at Zeppelin increased by a factor of three compared to 2017 to 2018 and in 2020 by a factor of nine, and thus for 2020 the annual mean at Zeppelin (1.15 ng m^{-3}) was nearly twice as high as the highest annual mean seen at Birkenes (0.610 ng m^{-3} in 2018).

The atmospheric lifetime of isoprene is < 4 hours, whereas the lifetime of 2-methyltetrols is unknown (Wennberg et al., 2018) and the amount attributed to formation from locally emitted isoprene vs. LRT 2-methyltetrols remains an open question. The 2-methyltetrols level at Birkenes increase by nearly a factor of 20 when leaves unfold in May (Yttri et al., 2021). Consequently, the effect of leaves unfolding 0.5 to 1.5 months earlier in continental Europe (the leaves of *Betula Pubescens* unfold 2.1 days later pr. 100 km along a South to North transect in Europe; Rötzer and Chmielewski, 2001) does not seem to have an influence, suggesting that the 2-methyltetrols level largely reflect local formation. At Svalbard, there are no forests, and hardly any trees, still there is vegetation (including mosses and lichens) that emit isoprene, that can have emission rates that are considerably higher than those observed at Southern latitudes (Kramshøj, et al., 2016). Circumpolar land masses are situated further away from Zeppelin than continental Europe from Birkenes, thus local formation of 2-methyltetrols might be important also at Svalbard. Marine sources of isoprene cannot be excluded, particularly in remote marine areas (Liakakou et al., 2007), although macro algae seem to favor dimethyl sulfide (DMS) formation rather than isoprene in the Arctic (Dani and Loreto, 2017). Further, time series of 2-methyltetrols and MSA at Zeppelin (Sharma et al., 2012) do not co-vary, suggesting a non-marine origin of 2-methyltetrols.

The increased 2-methyltetrol level at Zeppelin in 2019 to 2020 occurred during summer. From 30 June to 11 of August 2020, weekly mean concentrations ranged from 5.9 to 28 ng m^{-3} for four out of

six weeks, being up to five times higher than the highest weekly mean at Birkenes (5.6 ng m^{-3}) for 2017 to 2018. We recognize that levoglucosan was elevated (1.0 to 6.0 ng m^{-3}) for these four weeks and that air masses were influenced by WF emissions in Western Russia (Fig. 7; Sect. 3.5.1). We are left speculating how WF might have augmented 2-methyltetrol levels. Isoprene emissions are enhanced by increased temperature and a fire plume provides favorable conditions for BSOA formation and aerosol surface area for condensation. Notably, 2-methyltetrols are semi volatile (Lopez-Hilfiker et al., 2016) and at high OA loadings increased partitioning to the aerosol phase will occur. Further, transport time was short (Fig. S3), which is favorable concerning potential degradation of 2-methyltetrols. Increased formation from local isoprene emissions is likely, as ambient temperature at Zeppelin was unprecedentedly high in this period (See Sect 3.5.1 and Fig. 7 for details). The elevated 2-methyltetrol concentration (3.7 ng m^{-3}) seen for the warm period in the beginning of July 2019 was not nearly as high as for July and August 2020 and levoglucosan (0.04 ng m^{-3}) was not increased.

2-methyltetrols (here: ng C m^{-3}) contributed up to 0.34% to OC monthly in the NH-season in 2019 and 0.56% in 2020, being clearly higher compared to the two previous years (0.14% and 0.23%), which in turn was higher than the highest monthly means at Birkenes (0.09% and 0.12%). Compared to rural central Europe (0.68% in June) (Ion et al., 2005) and Boreal Forest Finland (0.88% in the July to August transition) (Kourtchev et al., 2005), the highest contributions at Zeppelin in 2020 are slightly lower.

Multi-year time series of 2-methyltetrols are rare, particularly in areas with low NO_x-concentrations (Noziere et al., 2011; Cui et al., 2018). We find that the NH-season drop in the 2-methylthreitol to 2-methylerythritol ratio was much more pronounced at Birkenes (0.36 ± 0.11) than at Zeppelin (0.54 ± 0.12) (Table S6). A NH-season drop is also observed the Hyytiälä Observatory (Boreal Forest Finland) (Kourtchev et al., 2005). Elevated ratios were observed at Zeppelin in July (0.83) and August (0.70) 2020 when influenced by WF emissions, being substantially higher compared to July – August (0.45 ± 0.04) of previous years. With the exceptions mentioned, the mean ratio for the NH-season at Zeppelin agrees with the upper range (0.25 to 0.58) reported by others (Claeys et al., 2010). This relates to the formation mechanism of 2-methylterols outlined by Bates et al. (2014), which shows a 1:2 relationship between *cis*-ß-IEPOX and *trans*-ß-IEPOX, accounting for >97% of observed IEPOX, and which are the precursors of 2-methylthreitol and 2-methylerythritol, respectively. Notably, 2-methyltetrols can also result from the degradation of IEPOX-derived organosulfates through hydrolysis of tertiary ones (Darer et al., 2011), however these species were not measured in the present study.

There are studies suggesting a biological (enzymatic) origin of 2-methyltetrols, as there is an enantiomer excess of both 2-C-methyl-D-erythritol and 2-C-methyl-threitol (Noziere et al., 2011; Gonzaléz et al., 2014; Jacobsen and Anthonsen, 2015). If the 2-methyltetrols formation was exclusively abiotic, resulting from atmospheric oxidation of isoprene (Claeys et al., 2004), there would be a racemic mixture of the 2-methyltetrols. This is consistent with the known production of the 2-methylerythritol D-form by plants, algae, and microorganisms (Anthonsen et al., 1976, 1980; Dittrich and Angyal, 1988;

Ahmed et al., 1996; Duvold et al., 1997; Sagner et al., 1998; Enomoto et al., 2004). Consequently, it can be questioned if 2-methyltetrols are exclusive tracers of BSOA from atmospheric oxidation of isoprene, e.g., a 30 to 67% biological contribution was calculated for May to December for the Aspvreten site (Sweden) (Noziere et al., 2011). Unfortunately, the analysis done in the present study does not allow for a proper investigation of a potential biological contribution. Cahill et al. (2006) argued for a biological source based on the correlation between 2-methyltetrol and the PBAP tracers glucose (r^2 = 0.732) and fructose (r^2 = 0.644) for eleven samples. At Zeppelin, r^2 for 2-methyltetrols vs. fructose (0.951), glucose (0.946) and arabitol (0.801) appears elevated in the NH-season but drops substantially (r^2 = 0.052 – 0.437) when excluding the extreme values in July and August 2020. At Birkenes, correlation was non-existing (r^2 = 0.000 – 0.025). Source apportionment of CA by PMF at Birkenes showed that the factor explaining 94% of the 2-methyltetrols explained only 6% of the PBAP tracers, and that the factor explaining 89% of the PBAP tracers explained only 2.5% of the 2-methyltetrols (Yttri et al., 2021). Hence, statistics do not argue for a common source of 2-methyltetrols, or a fraction of 2-methyltetrols, and PBAP tracers. Further, 2-methylerythritol vs. 2-methylthreitol correlated highly both at Zeppelin (r^2 = 0.971) and at Birkenes (r^2 = 0.889), suggesting one dominating source (abiotic secondary formation), corresponding to findings by El-Haddad et al. (2011). However, potential mechanisms by which biologically formed 2-methyltetrols are released to the atmosphere are not known, thus a biological contribution cannot be excluded.

3.4 Primary biological aerosol particles

The interest in PBAP has grown over the last two decades, with rising awareness of its contribution to the OA budget (e.g., Waked et al. 2014; Yttri et al. 2021; Moschos et al., 2022) and as a source of warm ice nucleating particles, deemed more important than cloud condensation nuclei regarding Arctic cloud radiative properties (Solomon et al., 2018). We address a handful of PBAP tracers, discuss their levels, seasonality, and sources, including cellulose, measured in Arctic aerosol for the first time.

3.4.1 Sugars and sugar-alcohols

Annual mean concentrations of sugars and sugar-alcohols were 1 to 2 orders of magnitude lower at Zeppelin compared to Birkenes, reflecting the modestly vegetated Arctic and that PBAP mainly have a local origin (Samaké et al., 2019). This contrasts with the factors for 2-methyltetrols (≤5), which are secondarily formed species with a stronger regional character but might also relate to the temperature sensitive high flux of biogenic volatile organic compounds for Arctic vegetation (Kramshøj et al., 2016). Higher levels of primary biological organic aerosol (PBOA) at Gruvebadet (50 m asl), one km south of Ny-Ålesund, compared to the Zeppelin Observatory (472 m asl) (Moschos et al., 2022) indicate a local contribution associated with the more verdant lower altitude areas. However, maximum concentrations of sugars and sugar-alcohols were observed for the LRT episode 22 – 27 July 2020 (Sect. 3.6.1), explaining 29% of the annual sugars and sugar-alcohols loading. We are left speculating about the LRT

fraction of PBAP vs. that of local origin, but LRT likely makes a larger contribution to PBAP in the Arctic than for more vegetated southerly biomes.

All species experienced a modest increase in June, coinciding with the onset of the growing season, but evolved differently after that, suggesting a mixture of sources, highlighting the importance of measuring a broad specter of PBAP tracers. Arabitol and mannitol were elevated throughout summer before successively declining towards the end of the year, fructose and glucose started decreasing immediately after the peak level in July, whereas trehalose experienced comparable levels from July to November. Snow cover can be decisive for PBAP levels (Yttri et al., 2007 a, b) and probably more so for the non-forested Arctic. However, our data does not explicitly demonstrate an influence of the snow cover, e.g., the seasonality of trehalose (and cellulose; Sect 3.4.2).

The composition of sugars and sugar-alcohols at Zeppelin (Table 1) and Birkenes (Table S5) varied, reflecting different biomes. Glucose was the most abundant sugar regardless of the season at Zeppelin. At Birkenes, glucose dominated only in winter, while arabitol and mannitol were more prominent in summer. Trehalose levels were comparable or slightly higher than arabitol and mannitol at Zeppelin but lower at Birkenes. Samaké et al. (2020) showed how only a few genera of fungi and bacteria were responsible for the sugar and sugar-alcohol containing PBAP in PM_{10} filter samples at a rural site in France, and that these were associated with leaves rather than soil material. This strong association between sugars and sugar-alcohols and vegetation likely explain the very low levels of these PBAP tracers at Zeppelin compared to Birkenes. Samaké et al. (2020) point to the fungus *Cladosporium sp*. when explaining ambient aerosol levels of arabitol, mannitol and trehalose, as does Yttri et al. (2007a) for Birkenes. The annual mean mannitol to arabitol ratio was comparable between Zeppelin (1.1 ± 0.5) and Birkenes (1.0 ± 0.0) (Table S6), and to values reported for the Nordic countries (Yttri et al., 2011b). Mannitol and arabitol were highly correlated in the NH-season (r^2 = 0.983) when levels were elevated, and mannitol to arabitol ratio variability minor, suggesting one common source dominating. However, four samples with a mannitol to arabitol ratio ≥ 3 in the April to May transition could indicate influence from another source. Mannitol is considered the most abundant naturally occurring polyol, present and produced in a wide range of living organisms (Tonon et al., 2017), accounting for 25% of the dry weight of macro algae for certain parts of the year (Horn et al., 2000), however, our data for Zeppelin suggest that fungal spores are decisive for arabitol and mannitol present in the Arctic aerosol. Assuming all mannitol was associated with fungal spores, their carbon content contributed 0.5 ± 0.2% to OC annually when applying the lower OC/mannitol ratio (5.2) of Bauer et al. (2002), whereas the highest monthly mean was seen for September (1.5 ± 1.2%). The contribution reached 5% for only two of the weekly samples. Using the higher OC/mannitol ratio (10.8), would double these estimates.

Glucose is a building block of natural dimers and polymers and a ubiquitous primary molecular energy source, and thus an important PBAP. Small amounts of glucose are present in RWC emissions (Nolte et al., 2001) and are increased in air masses influenced by forest fire smoke (Medeiros et al., 2006). Notably, nine of the ten samples highest in glucose were also highly increased with respect to

levoglucosan and were all collected in the NH-season (Table S8), demonstrating WF as an important source of glucose brought to the Arctic by LRT. A largely similar finding was made for the other sugars and sugar-alcohols. Previous studies do not seem to link fungal related sugars and sugar-alcohols (arabitol, mannitol, trehalose) with WF emissions (e.g., Table 5 in Medeiros et al., 2006), nor with RWC emissions, e.g., levoglucosan and sugar-alcohols end up in different factors in PMF studies (Waked et al., 2014; Yttri et al., 2021). This might partly be due to lack of correlation between levoglucosan and sugar-alcohols for an entire data set. Indeed, low correlations between levoglucosan and sugar-alcohols ($r^2_{NH\text{-}season} < 0.423$; $r^2_{H\text{-}season} < 0.056$) were obtained considering the entire data set for Zeppelin, although the data presented in Table S8 clearly demonstrates a connection between WF and sugar-alcohols.

We estimated a 7 – 15% contribution of PBAP to OC annually, using an OC-to-$PBAP_{Tracers}$ emission ratio (ER) of 14.6 ± 2.1 (Zwaaftink et al., 2022), derived from measurements in the Boreo-nemoral zone (Yttri et al., 2021), keeping in mind that such an ER would be site specific.

3.4.2 Cellulose

Cellulose was the most abundant organic tracer analyzed (annual mean concentration of 2.2 ± 0.6 ng m^{-3}), but levels were much lower than in rural areas of continental Europe (annual mean: 16.3 – 284 ng m^{-3}) (Sánchez-Ochoa et al., 2007; Brighty et al., 2022), likely due to sparse vegetation at Svalbard. The highest monthly means were seen for June followed by October, but there was no pronounced seasonality for cellulose as seen for the other PBAP tracers (Sect. 3.4.1). This corresponds with findings made by Sánchez-Ochoa et al. (2007) who pointed to a minor seasonality *"with higher winter levels than expected",* and that of Puxbaum and Tenze-Kunit (2003) who associated increased cellulose levels in spring with *"seed production and repulsing of other cellulose containing plant material",* and "*production of leaf litter"* in fall. High wind speed might be a driving force for generation and entrainment of cellulose containing aerosol particles that is more pronounced in winter, and particularly in the harsh Arctic climate, but possibly limited by snow cover. In the recent study by Brighty et al. (2022), a clear seasonality was shown with increased levels in summer and fall at French and Swiss rural sites.

Size distribution measurement of cellulose is limited and inconclusive, with highest concentrations reported both for the fine (Puxbaum and Tenze-Kunit, 2003) and the coarse mode (Yttri et al., 2011a; Brighty et al., 2022). Lack of comparable seasonality between nearby sites indicates that local sources dominate (Brighty et al., 2022), but with a certain fraction associated with fine aerosol, LRT is a possibility. Cellulose did not correlate with other PBAP tracers or levoglucosan, corresponding to the findings by Brighty et al. (2022), but this does not exclude co-emission (see Sect. 3.4.1). A minor fraction (0.08%) of RWC emissions was attributed to cellulose in a combustion study by Schmidl et al. (2008), but we found no strong connection between the samples highest in cellulose and levoglucosan, as we did for the other PBAP tracers and levoglucosan, nor between cellulose and the other PBAP tracers (Table S8). The lack of resemblance between cellulose and other PBAP tracers and BB aerosol should

be explored further.

Cellulose (here: ng C m^{-3}) made a 1.0 ± 0.3% contribution to OC annually, corresponding to the lower range reported for rural background sites along an east to west transect across Europe (0.7 – 3.9%) (Sánchez-Ochoa et al., 2007), but substantially lower compared to French (3.2 ± 2.4 %) and Swiss (5.9 ± 4.4%) rural background sites (Brighty et al., 2022).

The contribution of plant debris (here: ng C m^{-3}) was estimated from cellulose (Puxbaum and Tenze Kunit, 2003; Yttri et al., 2011a,b) as a 2.0 ± 0.6% contribution to OC annually, and thus somewhat higher than for fungal spores (0.5 – 1.1%). On a monthly basis, 4 to 6% contributions were observed in all seasons. Weekly samples (n = 23) with a high (5 to 12%) plant debris contribution were associated with low OC levels (mean: 53 ng C m^{-3}; 22 percentile). Plant debris and OC were correlated (r^2 = 0.707), suggesting that plant debris is a driver of observed OC levels at low concentrations. We did not observe a similar feature for fungal spores.

3.5 Source apportionment of carbonaceous aerosol by Latin Hypercube Sampling

Source apportionment of CA (here: TC) by the LHS approach showed that natural sources dominated in the NH-season (85%) and anthropogenic in the H-season (73%), assuming all biomass burning emissions originated from WF in the NH-season and from RWC in H-season (Fig. 5). Even without attributing BB emissions to WF, natural sources still dominated in the NH-season (60%).

BSOA (56%) was the most abundant natural source in the NH-season, then WF (26%) and PBAP (3.2%). Compared to previous studies (Yttri et al., 2011 a and b), we found a lower PBAP fraction, which we attributed to the less vegetated Arctic environment. Note that the LHS approach underestimate the PBAP fraction by only accounting for fungal spores and plant debris, apportioning a part of PBAP to BSOA (Yttri et al., 2021). The PBAP fraction increased to 11% when using an OC-to-$PBAP_{Tracers}$ emission ratio (ER) of 14.6 ± 2.1 (Zwaaftink et al., 2022) including the sum of arabitol, mannitol, glucose, and trehalose. Note that this ER was obtained from measurements in the boreo-nemoral zone, and thus more representative of LRT than local PBAP sources.

RWC (46%) was the major fraction in the H-season followed by FF (27%) and BSOA (25%), whereas PBAP (1.4%) was negligible, even when considering the upper estimate (2.7%) obtained using the ER by (Zwaaftink et al., 2022). The absence of 2-methyltetrols in winter indicated that BSOA was formed from oxidation of mono- and sesquiterpenes and dimethyl sulfide, which seem more abundant in the Arctic winter than oxidation products of isoprene (Fu et al., 2009a; Sharma et al., 2012). Further, modelling studies suggest that increased condensation may explain wintertime BSOA (Simpson et al., 2007), which might be particularly relevant for the low Arctic temperatures.

Our source apportionment results for Zeppelin aligns with findings from rural background sites in Europe (e.g., Gelencsér et al., 2007; Genberg et al., 2011; Gilardoni et al., 2011; Glasius et al. 2017; Yttri et al., 2011a), where RWC dominates during the H-season and BSOA dominate in the NH-season. Rerunning the analysis using levoglucosan instead of ^{14}C-EC for apportionment of BB emissions,

lowered the contribution from WF in the NH-season from 26% to 4.4%. However, the contribution from natural sources remained consistent, as BSOA accounted for the modern carbon redistributed from WF. In the H-season, the contribution from RWC decreased from 46% to 8.9%, making BSOA (62%) and natural sources (64%) the major fractions even in the H-season. Hence, the choice of tracer (levoglucosan vs. ^{14}C-EC) would lead to different results and conclusions for Zeppelin.

3.6 LRT episodes outside the AH period

LRT episodes are decisive for CA levels and seasonality observed at Zeppelin. We analyzed in detail the three episodes with the highest weekly means of OC, which also had three of the four highest weekly means of EC (Figs. 6 to 8). All these episodes had air masses originating from NW Eurasia.

3.6.1 Episode 1 (22 July to 27 July 2020) – WF, BSOA, and PBAP

In transition July to August 2020, CA levels were high, with peak concentrations from 22 – 27 July (2172 ng C m^{-3} for OC and 59 µg C m^{-3} for EC). These levels were the highest in four years of observations, explaining 21% of the annual OC loading, but only 7% of EC. However, levels were still lower than the record high concentrations (3.5 µg C m^{-3} for OC and 0.24 µg C m^{-3} for EC) observed in the April to May transition 2006, caused by emissions from wild and agricultural fires in Eastern Europe (Stohl et al., 2007). All tracers (except cellulose) experienced maximum values during this episode, but 2-methyltetrols, glucose, fructose, and arabitol were the most elevated when compared to the long-term annual mean and to the enhancement seen for OC. The FLEXPART footprint clearly shows an influence from WF in the Khanty-Mansi district (Western Russia) (Fig. 7), corroborating to the high levoglucosan concentration (6.0 ng m^{-3}). Source apportionment by PMF attributed 55% of eBC to BB, whereas FLEXPART calculated 62%, with WF (95%) as the totally dominating fraction. Flaring was the dominating fossil fuel source category according to FLEXPART, explaining 58% of BC from fossil fuel sources.

The plume transport time from the source region to the Zeppelin Observatory was short; less than 7 days for 67% of eBC observed at Zeppelin 25 to 27 of July (Fig. S3), whereas on average only 30% of the observed eBC reaches the Arctic station after such short time. This might have contributed to the high level of 2-methyltetrols, which are indicated to have short atmospheric lifetimes (Yttri et al., 2021), in addition to the arguments raised in section 3.3. Certain PBAP, such as fungal spores (Bauer et al., 2002; Yttri et al., 2007a) are small enough to be transported over long distances, even between continents (Prospero et al., 2005), and pyro convection might bring larger sized PBAP to altitudes that enables LRT (e.g., Zwaaftink et al., 2022). PBAP contributed 14% of OC, using the OC-to-$PBAP_{Tracers}$ ER by Zwaaftink et al. (2022).

The high CA level coincided with a prolonged period (24 to 29 July) of high temperatures, unprecedented since temperature measurements were initiated at Zeppelin (1998), caused by intrusions of warm air masses from Siberia; T > 10 °C for 111 consecutive hours, mean T = 14.5 ± 1.5 °C, and

817 T_{Max} = 18.2 ºC. A disproportionally strong warming of the Arctic compared to the midlatitudes could
818 create an important pathway of pollution to the Arctic (Stohl et al. 2007), and as for the LRT episode in
819 spring 2006 (Stohl et al., 2007), emissions from WF at lower latitudes were essential in the deterioration
820 of Arctic air quality also in July 2020.
821
822 **3.6.2 Episode 2 (28 Sep to 6 Oct 2017) – A bit of everything**
823 Air masses with a history over south-western Russia, eastern, central, and northern Europe (including
824 Scandinavia) (Fig. 8) increased the OC (549 ng C m^{-3}) and EC (52 ng C m^{-3}) concentrations at Zeppelin
825 to levels corresponding to 14% of their annual loading. Source apportionment by the LHS suggested
826 that BSOA (57%) and BB (32%) dominated CA (Table S4). Certain PBAP tracers (arabitol, mannitol
827 and trehalose) were enhanced beyond that of OC, reflecting the seasonal peak in fungal spores, but
828 PBAP contributed only 3% to CA (Table S4). An upper estimate of 13% was obtained using the OC-to-
829 $PBAP_{Tracers}$ ER by Zwaaftink et al. (2022). PMF apportioned 47% of eBC to BB, comparing well with
830 FLEXPART (51%), (ascribing 62% of BB to WF) and LHS (58%). FLEXPART apportioned the
831 majority of BC from FF combustion to traffic (55%). The mean ambient temperature during the episode
832 was enhanced compared to the long-term mean, as seen for all three episodes described.
833
834 **3.6.3 Episode 3 (2 to 10 Oct 2020) – Wildfires and mineral dust**
835 This episode was studied by Zwaaftink et al. (2022), combining surface and remote sensing
836 observations and transport model simulations to understand its origin and development, whereas we in
837 the present study focused on its carbonaceous aerosol content. Briefly, the EC level (78 ng C m^{-3}) was
838 the highest in four years of observations, whereas the OC level (818 ng C m^{-3}) was much lower than
839 observations made during the July 2020 (Sect 3.5.1) episode, explaining 15% and 13% of the annual
840 EC and OC loading, respectively (Fig. 9). Levoglucosan (5.0 ng m^{-3}) was the only organic tracer
841 elevated beyond that of OC, supporting FLEXPART calculations pointing to WF emissions in Ukraine
842 and southern Russia, as one of two major sources of air pollution for this episode. Source
843 apportionment of eBC by PMF indicated an almost equal share of eBC from BB (52%) and FF
844 combustion (48%), as do FLEXPART (BB = 57% and FF = 43%), with the majority of BB attributed
845 to WF (72%), and traffic being the major FF category (52%). Mixing with mineral dust emissions
846 from Central Asia én route, caused a mineral dust level of 1.9 – 2.6 µg m^{-3}, likely explaining the
847 presence of carbonate (20 ng C m^{-3}; 100 ng CO_3^{2-} m^{-3}). Before entering the Arctic, the polluted air
848 masses deteriorated the air-quality in a large part of northern Europe, giving PM_{10} levels around 100
849 µg m^3, and the same aerosol particle chemical signature as described for Zeppelin. These levels violate
850 EU air quality guidelines, which have daily mean limit values for PM_{10} of 50 µg m^{-3}.
851
852 **4 Implications**
853 Lack of long-term OA measurements has been a limitation for understanding Arctic aerosol mass

closure. Further, OA speciation needed for source attribution and for studying impact on cloud condensation nuclei and ice nucleating particles are scarce. Our four-years study at Zeppelin Observatory at Svalbard shed light on some of these topics, demonstrating that OA is a significant fraction of the Arctic PM_{10} aerosol particle mass, though less than sea salt aerosol and mineral dust, as well as typically non-sea salt SO_4^{2-}. LRT episodes in the non-heating season dominated by natural emissions and their impact on OA levels, seasonality, and composition received particular focus, showing that WF also contribute to high BSOA and PBAP levels in the Arctic environment. The fraction of OA attributed to local sources vs. LRT is uncertain, particularly when experiencing intrusions of warm air masses from Siberia, as certain Arctic vegetation species have highly temperature sensitive biogenic volatile organic compounds emission rates. Arctic CA shares the same feature as CA in source regions in the mid latitudes (e.g., Gelencsér et al., 2007), i.e., natural sources, particularly BSOA, dominating in the non-heating season and anthropogenic emissions, predominantly RWC, in the heating season. The nine-fold increase in 2-methyltetrols observed for 2020 could be a harbinger of CA from natural sources increasing in the Arctic.

Contrary to both previous (Stohl et al., 2013; Winiger et al., 2019) and present (this study) modeling and radiocarbon studies, PMF did not predict WF as the major source of eBC at Zeppelin Observatory in the non-heating season. However, the predominant role of BC from WF emissions at Northern latitudes stated by McCarty et al. (2021) was neither reflected by PMF nor by FLEXPART for 2017 to 2020. This calls for an investigation of whether the stated increase in BC from WF emissions for 2010 – 2020 at Northern latitudes (McCarty et al., 2021) is reflected at Arctic ground level. Up to two decades of stored multi wavelength aethalometer data for Arctic observatories, combined with the outlined PMF approach enables such a trend study. Additionally, a pan-Arctic investigation is encouraged for studying the spatial variability in eBC_{BB} and eBC_{FF}, facilitated by the inexpensive, high time resolution multi wavelength Aethalometer measurements that are widespread across the Arctic observatories (EU Action on Black Carbon in the Arctic, 2019). Increased anthropogenic activity such as shipping oil and gas exploration in the Arctic, warrants further separation of eBC from FF combustion, which can be attempted using additional high time resolution data as input to our analysis. This appears particularly important for the flaring source, suggested by modelling to contribute 42% to the annual mean BC surface concentration in the Arctic (Stohl et al., 2013), which yet remains to be confirmed by observations.

Our study shows a wide variability amongst different methods in apportioning BC according to FF and BB, warranting further investigation for a reliable abatement of sources relevant for BC in the Arctic. Still, the high time resolution observational signal of eBC from BB and FF combustion derived from Aethalometer measurements provide a hitherto unused tool important for assessing Arctic BC.

Continuation of the actual time series at Zeppelin Observatory is suited for revealing potential changes in the relative source composition of Arctic CA, be it from altered transport or changes in emissions. It is of special interest to monitor the frequency and magnitude of WF, how BSOA and PBAP

concentrations develop, and if FF emissions change from increased anthropogenic activity in the Polar region.

Data availability

All data used in the present paper are open access and are available at http://ebas.nilu.no/ (NILU, 2023), except radiocarbon data, which are presented in Rauber et al. (2023).

Supplement

The supplement related to this article is available online at:

Author contributions

SMP, KEY, and WA were responsible for conceptualizing the study. KEY wrote the original draft of the paper. WAA, SE, and KEY produced the figures. AB was responsible for collection of aerosol filter samples. HG analysed the organic tracers, MR and SS did the radiocarbon measurements, and AK-G was responsible for the cellulose analysis. MF, KEY, CLM, and WA carried out data curation. NE and SE did the FLEXPART modelling, whereas DS and MAY did the LHS calculations. SMP and KEY undertook the formal analysis. JS, AG, and ZZ acquired resources. KT, CLM and WA acquired funding. All co-authors contributed to writing, reviewing, and editing the final article.

Competing interests:

The contact author has declared that none of the authors has any competing interests.

Acknowledgement

The Norwegian Ministry of Climate and Environment provided funding to establish the OC/EC and organic tracers time series used in the present study and are gratefully acknowledged. These data are reported to the EMEP monitoring programme and are available from the EBAS database infrastructure (http://ebas.nilu.no) hosted at NILU. The research leading to these results has benefited from the Aerosols, Clouds, and Trace gases Research InfraStructure (ACTRIS) network, funding from the European Union Seventh Framework Programme (FP7/2007–2013) under ACTRIS-2 and grant agreement no. 262254 (i.e., participation in inter-laboratory comparison for thermal–optical analysis and QA and QC of measurements. S.E. and N.E. received funding from AMAP and the ABC-iCAP project. Staff from the Norwegian Polar Institute are greatly acknowledged for changing of filters at the Zeppelin Observatory. A.G., Z.Z. and J.D.S. thank the US National Science Foundation (NSF) under Atmospheric and Geospace (AGS) Grant 2001027 for funding the synthesis of 2-methyltetrols used in this study. We used ChatGPT (3.5) to condense and improve the language of specific sections in the review process of this manuscript.

Financial support.

This research has been supported by the Norwegian Ministry of Climate and Environment.

References

Aas, W., Eckhardt, S., Fiebig, M., Solberg, S., and Yttri, K. E.: Monitoring of long-range transported air pollutants in Norway, annual report 2019, Miljødirektoratet rapport, NILU, Kjeller, Norway, M-1710/2020 NILU OR 4/2020, 2020.

Agrios, K., Salazar, G., Zhang, Y. L., Uglietti, C., Battaglia, M., Luginbuhl, M., Ciobanu, V. G., Vonwiller, M., and Szidat, S.: Online coupling of pure O-2 thermo-optical methods-C-14 AMS for source apportionment of carbonaceous aerosols, Nuclear Instruments & Methods in Physics Research Section B-Beam Interactions with Materials and Atoms, 361, 288-293, 10.1016/j.nimb.2015.06.008, 2015.

Ahmed, A. A., AbdElRazek, M. H., AbuMostafa, E. A., Williams, H. J., Scott, A. I., Reibenspies, J. H., and Mabry, T. J.: A new derivative of glucose and 2-C-methyl-D-erythritol from Ferula sinaica, Journal of Natural Products, 59, 1171-1173, 1996.

Akagi, S. K., Yokelson, R. J., Wiedinmyer, C., Alvarado, M. J., Reid, J. S., Karl, T., Crounse, J. D., and Wennberg, P. O.: Emission factors for open and domestic biomass burning for use in atmospheric models, Atmospheric Chemistry and Physics, 11, 4039-4072, 10.5194/acp-11-4039-2011, 2011.

Alastuey, A., Querol, X., Aas, W., Lucarelli, F., Perez, N., Moreno, T., Cavalli, F., Areskoug, H., Balan, V., Catrambone, M., Ceburnis, D., Cerro, J. C., Conil, S., Gevorgyan, L., Hueglin, C., Imre, K., Jaffrezo, J.-L., Leeson, S. R., Mihalopoulos, N., Mitosinkova, M., O'Dowd, C. D., Pey, J., Putaud, J.-P., Riffault, V., Ripoll, A., Sciare, J., Sellegri, K., Spindler, G., and Yttri, K. E.: Geochemistry of PM_{10} over Europe during the EMEP intensive measurement periods in summer 2012 and winter 2013, Atmospheric Chemistry and Physics, 16, 6107-6129, 10.5194/acp-16-6107-2016, 2016.

Anthonsen, T., Hagen, S., Kazi, M. A., Shah, S. W., and Tagar, S.: 2-C-methyl-erythritol, a new branched alditol from convolvulus-glomeratus, Acta Chemica Scandinavica Series B-Organic Chemistry and Biochemistry, 30, 91-93, 10.3891/acta.chem.scand.30b-0091, 1976.

Anthonsen, T., Hagen, S., and Sallam, M.A.E.: Synthetic and spectroscopic studies of 2-C-methyl-erythritol and 2-C-methyl-threitol, Phytochemistry, 19, 2375-2377, 10.1016/s0031-9422(00)91030-6, 1980.

Barrett, T. E., Robinson, E. M., Usenko, S., and Sheesley, R. J.: Source Contributions to Wintertime Elemental and Organic Carbon in the Western Arctic Based on Radiocarbon and Tracer Apportionment, Environmental Science & Technology, 49, 11631-11639, 10.1021/acs.est.5b03081, 2015.

Barrett, T. E., and Sheesley, R. J.: Year-round optical properties and source characterization of Arctic organic carbon aerosols on the North Slope Alaska, Journal of Geophysical Research-Atmospheres, 122, 9319-9331, 10.1002/2016jd026194, 2017.

Bates, K. H., Crounse, J. D., St Clair, J. M., Bennett, N. B., Nguyen, T. B., Seinfeld, J. H., Stoltz, B. M., and Wennberg, P. O.: Gas Phase Production and Loss of Isoprene Epoxydiols, Journal of Physical Chemistry A, 118, 1237-1246, 10.1021/jp4107958, 2014.

Bauer, H., Kasper-Giebl, A., Loflund, M., Giebl, H., Hitzenberger, R., Zibuschka, F., and Puxbaum, H.: The contribution of bacteria and fungal spores to the organic carbon content of cloud water, precipitation and aerosols, Atmospheric Research, 64, 109-119, 10.1016/s0169-8095(02)00084-4, 2002.

971 Bond, T. C., Doherty, S. J., Fahey, D. W., Forster, P. M., Berntsen, T., DeAngelo, B. J., Flanner, M. G.,
972 Ghan, S., Karcher, B., Koch, D., Kinne, S., Kondo, Y., Quinn, P. K., Sarofim, M. C., Schultz, M. G.,
973 Schulz, M., Venkataraman, C., Zhang, H., Zhang, S., Bellouin, N., Guttikunda, S. K., Hopke, P. K.,
974 Jacobson, M. Z., Kaiser, J. W., Klimont, Z., Lohmann, U., Schwarz, J. P., Shindell, D., Storelvmo, T.,
975 Warren, S. G., and Zender, C. S.: Bounding the role of black carbon in the climate system: A scientific
976 assessment, Journal of Geophysical Research-Atmospheres, 118, 5380-5552, 10.1002/jgrd.50171, 2013.

977 Brighty, A., Jacob, V., Uzu, G., Borlaza, L., Conil, S., Hueglin, C., Grange, S. K., Favez, O., Trebuchon,
978 C., and Jaffrezo, J. L.: Cellulose in atmospheric particulate matter at rural and urban sites across France
979 and Switzerland, Atmospheric Chemistry and Physics, 22, 6021-6043, 10.5194/acp-22-6021-2022,
980 2022.

981 Cahill, T. M., Seaman, V. Y., Charles, M. J., Holzinger, R., and Goldstein, A. H.: Secondary organic
982 aerosols formed from oxidation of biogenic volatile organic compounds in the Sierra Nevada Mountains
983 of California, Journal of Geophysical Research-Atmospheres, 111, 10.1029/2006jd007178, 2006.

984 Cassiani, M., Stohl, A., and Brioude, J.: Lagrangian Stochastic Modelling of Dispersion in the
985 Convective Boundary Layer with Skewed Turbulence Conditions and a Vertical Density Gradient:
986 Formulation and Implementation in the FLEXPART Model, Boundary-Layer Meteorology, 154, 367-
987 390, 10.1007/s10546-014-9976-5, 2015.

988 Cavalli, F., Viana, M., Yttri, K. E., Genberg, J., and Putaud, J.-P.: Toward a standardised thermal-optical
989 protocol for measuring atmospheric organic and elemental carbon: the EUSAAR protocol, Atmospheric
990 Measurement Techniques, 3, 79-89, 2010.

991 Cavalli, F., Alastuey, A., Areskoug, H., Ceburnis, D., Cech, J., Genberg, J., Harrison, R. M., Jaffrezo,
992 J. L., Kiss, G., Laj, P., Mihalopoulos, N., Perez, N., Quincey, P., Schwarz, J., Sellegri, K., Spindler, G.,
993 Swietlicki, E., Theodosi, C., Yttri, K. E., Aas, W., and Putaud, J. P.: A European aerosol
994 phenomenology-4: Harmonized concentrations of carbonaceous aerosol at 10 regional background sites
995 across Europe, Atmospheric Environment, 144, 133-145, 10.1016/j.atmosenv.2012.07.050, 2016.

996 Claeys, M., Graham, B., Vas, G., Wang, W., Vermeylen, R., Pashynska, V., Cafmeyer, J., Guyon, P.,
997 Andreae, M. O., Artaxo, P., and Maenhaut, W.: Formation of secondary organic aerosols through
998 photooxidation of isoprene, Science, 303, 1173-1176, 10.1126/science.1092805, 2004.

999 Claeys, M., Kourtchev, I., Pashynska, V., Vas, G., Vermeylen, R., Wang, W., Cafmeyer, J., Chi, X.,
1000 Artaxo, P., Andreae, M. O., and Maenhaut, W.: Polar organic marker compounds in atmospheric
1001 aerosols during the LBA-SMOCC 2002 biomass burning experiment in Rondonia, Brazil: sources and
1002 source processes, time series, diel variations and size distributions, Atmospheric Chemistry and Physics,
1003 10, 9319-9331, 10.5194/acp-10-9319-2010, 2010.

1004 Clarke, A. D., and Noone, K. J.: Soot in the Arctic snowpack - A cause for perturbations in radiative-
1005 transfer, Atmospheric Environment, 19, 2045-2053, 10.1016/0004-6981(85)90113-1, 1985.

1006 Coen, M. C., Andrews, E., Alastuey, A., Arsov, T. P., Backman, J., Brem, B. T., Bukowiecki, N., Couret,
1007 C., Eleftheriadis, K., Flentje, H., Fiebig, M., Gysel-Beer, M., Hand, J. L., Hoffer, A., Hooda, R.,
1008 Hueglin, C., Joubert, W., Keywood, M., Kim, J. E., Kim, S. W., Labuschagne, C., Lin, N. H., Lin, Y.,
1009 Myhre, C. L., Luoma, K., Lyamani, H., Marinoni, A., Mayol-Bracero, O. L., Mihalopoulos, N., Pandolfi,
1010 M., Prats, N., Prenni, A. J., Putaud, J. P., Ries, L., Reisen, F., Sellegri, K., Sharma, S., Sheridan, P.,
1011 Sherman, J. P., Sun, J. Y., Titos, G., Torres, E., Tuch, T., Weller, R., Wiedensohler, A., Zieger, P., and
1012 Laj, P.: Multidecadal trend analysis of in situ aerosol radiative properties around the world, Atmospheric
1013 Chemistry and Physics, 20, 8867-8908, 10.5194/acp-20-8867-2020, 2020.

Creamean, J. M., Kirpes, R. M., Pratt, K. A., Spada, N. J., Maahn, M., de Boer, G., Schnell, R. C., and China, S.: Marine and terrestrial influences on ice nucleating particles during continuous springtime measurements in an Arctic oilfield location, Atmospheric Chemistry and Physics, 18, 18023-18042, 10.5194/acp-18-18023-2018, 2018.

Creamean, J. M., Mignani, C., Bukowiecki, N., and Conen, F.: Using freezing spectra characteristics to identify ice-nucleating particle populations during the winter in the Alps, Atmospheric Chemistry and Physics, 19, 8123-8140, 10.5194/acp-19-8123-2019, 2019.

Creamean, J. M., Hill, T. C. J., DeMott, P. J., Uetake, J., Kreidenweis, S., and Douglas, T. A.: Thawing permafrost: an overlooked source of seeds for Arctic cloud formation, Environmental Research Letters, 15, 10.1088/1748-9326/ab87d3, 2020.

Creamean, J. M., Barry, K., Hill, T. C., Hume, C., DeMott, P. J., Shupe, M. D., Dahlke, S., Willmes, S., Schmale, J., Beck, I., Hoppe, C. J. M., Fong, A., Chamberlain, E., Bowman, J., Scharien, R., and Persson, O.: Annual cycle observations of aerosols capable of ice formation in central Arctic clouds, Nat. Commun., 13, 1–12, 2022.

Cui, T. Q., Zeng, Z. X., dos Santos, E. O., Zhang, Z. F., Chen, Y. Z., Zhang, Y., Rose, C. A., Budisulistiorini, S. H., Collins, L. B., Bodnar, W. M., de Souza, R. A. F., Martin, S. T., Machado, C. M. D., Turpin, B. J., Gold, A., Ault, A. P., and Surratt, J. D.: Development of a hydrophilic interaction liquid chromatography (HILIC) method for the chemical characterization of water-soluble isoprene epoxydiol (IEPOX)-derived secondary organic aerosol, Environmental Science-Processes & Impacts, 20, 1524-1536, 10.1039/c8em00308d, 2018.

Dani, K. G. S., and Loreto, F.: Trade-Off Between Dimethyl Sulfide and Isoprene Emissions from Marine Phytoplankton, Trends in Plant Science, 22, 361-372, 10.1016/j.tplants.2017.01.006, 2017.

Darer, A. I., Cole-Filipiak, N. C., O'Connor, A. E., Elrod, M. J.: Formation and Stability of Atmospherically Relevant Isoprene-Derived Organosulfates and Organonitrates, Environ. Sci. Technol. 45 (5), 1895 – 1902, https://doi.org/10.1021/es103797z, 2011.

Dittrich, P., and Angyal, S. J.: 2-C-methyl-erythritol in leaves of Liriodendron-tulipifera, Phytochemistry, 27, 935-935, 10.1016/0031-9422(88)84125-6, 1988.

Duvold, T., Bravo, J. M., PaleGrosdemange, C., and Rohmer, M.: Biosynthesis of 2-C-methyl-D-erythritol, a putative C-5 intermediate in the mevalonate independent pathway for isoprenoid biosynthesis, Tetrahedron Letters, 38, 4769-4772, 10.1016/s0040-4039(97)01045-9, 1997.

Dye, C., and Yttri, K.: Determination of monosaccharide anhydrides in atmospheric aerosols by use of high-performance liquid chromatography combined with high-resolution mass spectrometry, Analytical Chemistry, 77, 1853-1858, 10.1021/ac049461j, 2005.

Elbert, W., Taylor, P. E., Andreae, M. O., and Poschl, U.: Contribution of fungi to primary biogenic aerosols in the atmosphere: wet and dry discharged spores, carbohydrates, and inorganic ions, Atmospheric Chemistry and Physics, 7, 4569-4588, 10.5194/acp-7-4569-2007, 2007.

El Haddad, I., Marchand, N., Temime-Roussel, B., Wortham, H., Piot, C., Besombes, J. L., Baduel, C., Voisin, D., Armengaud, A., and Jaffrezo, J. L.: Insights into the secondary fraction of the organic aerosol in a Mediterranean urban area: Marseille, Atmospheric Chemistry and Physics, 11, 2059-2079, 10.5194/acp-11-2059-2011, 2011.

Eleftheriadis, K., Vratolis, S., and Nyeki, S.: Aerosol black carbon in the European Arctic: Measurements at Zeppelin station, Ny-Alesund, Svalbard from 1998-2007, Geophysical Research Letters, 36, 10.1029/2008gl035741, 2009.

Enomoto, H., Kohata, K., Nakayama, M., Yamaguchi, Y., and Ichimura, K.: 2-C-methyl-D-erythritol is a major carbohydrate in petals of Phlox subulata possibly involved in flower development, Journal of Plant Physiology, 161, 977-980, 10.1016/j.jplph.2004.01.009, 2004.

EU Action on Black Carbon in the Arctic: Review of Observation Capacities and Data Availability for Black Carbon in the Arctic Region: EU Action on Black Carbon in the Arctic – Technical Report 1. 35 pp. https://www.amap.no/work-area/document/3058, 2019

Feltracco, M., Barbaro, E., Tedeschi, S., Spolaor, A., Turetta, C., Vecchiato, M., Morabito, E., Zangrando, R., Barbante, C., and Gambaro, A.: Interannual variability of sugars in Arctic aerosol: Biomass burning and biogenic inputs, Science of the Total Environment, 706, 10.1016/j.scitotenv.2019.136089, 2020.

Ferrero, L., Sangiorgi, G., Perrone, M. G., Rizzi, C., Cataldi, M., Markuszewski, P., Pakszys, P., Makuch, P., Petelski, T., Becagli, S., Traversi, R., Bolzacchini, E., and Zielinski, T.: Chemical Composition of Aerosol over the Arctic Ocean from Summer ARctic EXpedition (AREX) 2011-2012 Cruises: Ions, Amines, Elemental Carbon, Organic Matter, Polycyclic Aromatic Hydrocarbons, n-Alkanes, Metals, and Rare Earth Elements, Atmosphere, 10, 10.3390/atmos10020054, 2019.

Forster, C., Stohl, A., and Seibert, P.: Parameterization of convective transport in a Lagrangian particle dispersion model and its evaluation, Journal of Applied Meteorology and Climatology, 46, 403-422, 10.1175/jam2470.1, 2007.

Freitas, G.P., Adachi, K., Conen, F., Heslin-Rees, D., Krejci, R., Tobo, Y., Yttri, K.E. and Zieger, P. Regionally sourced bioaerosols drive high-temperature ice nucleating particles in the Arctic. Nat Commun 14, 5997 (2023). https://doi.org/10.1038/s41467-023-41696-7

Fu, P. Q., Kawamura, K., Chen, J., and Barrie, L. A.: Isoprene, Monoterpene, and Sesquiterpene Oxidation Products in the High Arctic Aerosols during Late Winter to Early Summer, Environmental Science & Technology, 43, 4022-4028, 10.1021/es803669a, 2009a.

Fu, P. Q., Kawamura, K., and Barrie, L. A.: Photochemical and Other Sources of Organic Compounds in the Canadian High Arctic Aerosol Pollution during Winter-Spring, Environmental Science & Technology, 43, 286-292, 10.1021/es803046q, 2009b.

Fu, P. Q., Kawamura, K., Kanaya, Y., and Wang, Z. F.: Contributions of biogenic volatile organic compounds to the formation of secondary organic aerosols over Mt Tai, Central East China, Atmospheric Environment, 44, 4817-4826, 10.1016/j.atmosenv.2010.08.040, 2010.

Fu, P. Q., Kawamura, K., Chen, J., Charriere, B., and Sempere, R.: Organic molecular composition of marine aerosols over the Arctic Ocean in summer: contributions of primary emission and secondary aerosol formation, Biogeosciences, 10, 653-667, 10.5194/bg-10-653-2013, 2013.

Garg, S., Chandra, B. P., Sinha, V., Sarda-Esteve, R., Gros, V., and Sinha, B.: Limitation of the Use of the Absorption Angstrom Exponent for Source Apportionment of Equivalent Black Carbon: a Case Study from the North West Indo-Gangetic Plain, Environmental Science & Technology, 50, 814-824, 10.1021/acs.est.5b03868, 2016

Gelencser, A., May, B., Simpson, D., Sanchez-Ochoa, A., Kasper-Giebl, A., Puxbaum, H., Caseiro, A., Pio, C., and Legrand, M.: Source apportionment of PM2.5 organic aerosol over Europe:

1096 Primary/secondary, natural/anthropogenic, and fossil/biogenic origin, Journal of Geophysical Research-
1097 Atmospheres, 112, 10.1029/2006jd008094, 2007.

1098 Genberg, J., Hyder, M., Stenstrom, K., Bergstrom, R., Simpson, D., Fors, E. O., Jonsson, J. A., and
1099 Swietlicki, E.: Source apportionment of carbonaceous aerosol in southern Sweden, Atmospheric
1100 Chemistry and Physics, 11, 11387-11400, 10.5194/acp-11-11387-2011, 2011.

1101 Giglio, L., Descloitres, J., Justice, C. O., and Kaufman, Y. J.: An enhanced contextual fire detection
1102 algorithm for MODIS, Remote Sensing of Environment, 87, 273-282, 10.1016/s0034-4257(03)00184-
1103 6, 2003.

1104 Gilardoni, S., Vignati, E., Cavalli, F., Putaud, J. P., Larsen, B. R., Karl, M., Stenstrom, K., Genberg, J.,
1105 Henne, S., and Dentener, F.: Better constraints on sources of carbonaceous aerosols using a combined
1106 C-14 - macro tracer analysis in a European rural background site, Atmospheric Chemistry and Physics,
1107 11, 5685-5700, 10.5194/acp-11-5685-2011, 2011.

1108 Glasius, M., Hansen, A. M. K., Claeys, M., Henzing, J. S., Jedynska, A. D., Kasper-Giebl, A., Kistler,
1109 M., Kristensen, K., Martinsson, J., Maenhaut, W., Nojgaard, J. K., Spindler, G., Stenstrom, K. E.,
1110 Swietlicki, E., Szidat, S., Simpson, D., and Yttri, K. E.: Composition and sources of carbonaceous
1111 aerosols in Northern Europe during winter, Atmospheric Environment, 173, 127-141,
1112 10.1016/j.atmosenv.2017.11.005, 2018.

1113 Gonzalez, N. J. D., Borg-Karlson, A. K., Artaxo, P., Guenther, A., Krejci, R., Noziere, B., and Noone,
1114 K.: Primary and secondary organics in the tropical Amazonian rainforest aerosols: chiral analysis of 2-
1115 methyltetraols, Environmental Science-Processes & Impacts, 16, 1413-1421, 10.1039/c4em00102h,
1116 2014.

1117 Graham, B., Guyon, P., Taylor, P. E., Artaxo, P., Maenhaut, W., Glovsky, M. M., Flagan, R.C., and
1118 Andreae, M. O.: Organic compounds present in the natural Amazonian aerosol: Character- ization by
1119 gas chromatography-mass spectrometry, J. Geophys. Res., 108, 4766, doi:10.1029/2003JD003990,
1120 2003.

1121 Grythe, H., Kristiansen, N. I., Zwaaftink, C. D. G., Eckhardt, S., Strom, J., Tunved, P., Krejci, R., and
1122 Stohl, A.: A new aerosol wet removal scheme for the Lagrangian particle model FLEXPART v10,
1123 Geoscientific Model Development, 10, 1447-1466, 10.5194/gmd-10-1447-2017, 2017.

1124 Hallquist, M., Wenger, J. C., Baltensperger, U., Rudich, Y., Simpson, D., Claeys, M., Dommen, J.,
1125 Donahue, N. M., George, C., Goldstein, A. H., Hamilton, J. F., Herrmann, H., Hoffmann, T., Iinuma,
1126 Y., Jang, M., Jenkin, M. E., Jimenez, J. L., Kiendler-Scharr, A., Maenhaut, W., McFiggans, G., Mentel,
1127 T. F., Monod, A., Prevot, A. S. H., Seinfeld, J. H., Surratt, J. D., Szmigielski, R., and Wildt, J.: The
1128 formation, properties and impact of secondary organic aerosol: current and emerging issues,
1129 Atmospheric Chemistry and Physics, 9, 5155-5236, 10.5194/acp-9-5155-2009, 2009.

1130 Hansen, A. M. K., Kristensen, K., Nguyen, Q. T., Zare, A., Cozzi, F., Nojgaard, J. K., Skov, H., Brandt,
1131 J., Christensen, J. H., Strom, J., Tunved, P., Krejci, R., and Glasius, M.: Organosulfates and organic
1132 acids in Arctic aerosols: speciation, annual variation and concentration levels, Atmospheric Chemistry
1133 and Physics, 14, 7807-7823, 10.5194/acp-14-7807-2014, 2014.

1134 Hansen, J., and Nazarenko, L.: Soot climate forcing via snow and ice albedos, Proceedings of the
1135 National Academy of Sciences of the United States of America, 101, 423-428,
1136 10.1073/pnas.2237157100, 2004.

Hartmann, M., Blunier, T., Brugger, S. O., Schmale, J., Schwikowski, M., Vogel, A., Wex, H., and Stratmann, F.: Variation of Ice Nucleating Particles in the European Arctic Over the Last Centuries, Geophysical Research Letters, 46, 4007-4016, 10.1029/2019gl082311, 2019.

Hartmann, M., Adachi, K., Eppers, O., Haas, C., Herber, A., Holzinger, R., Hunerbein, A., Jakel, E., Jentzsch, C., van Pinxteren, M., Wex, H., Willmes, S., and Stratmann, F.: Wintertime Airborne Measurements of Ice Nucleating Particles in the High Arctic: A Hint to a Marine, Biogenic Source for Ice Nucleating Particles, Geophysical Research Letters, 47, 10.1029/2020gl087770, 2020.

Hersbach, H., Bell, B., Berrisford, P., Hirahara, S., Horanyi, A., Munoz-Sabater, J., Nicolas, J., Peubey, C., Radu, R., Schepers, D., Simmons, A., Soci, C., Abdalla, S., Abellan, X., Balsamo, G., Bechtold, P., Biavati, G., Bidlot, J., Bonavita, M., De Chiara, G., Dahlgren, P., Dee, D., Diamantakis, M., Dragani, R., Flemming, J., Forbes, R., Fuentes, M., Geer, A., Haimberger, L., Healy, S., Hogan, R. J., Holm, E., Janiskova, M., Keeley, S., Laloyaux, P., Lopez, P., Lupu, C., Radnoti, G., de Rosnay, P., Rozum, I., Vamborg, F., Villaume, S., and Thepaut, J. N.: The ERA5 global reanalysis, Quarterly Journal of the Royal Meteorological Society, 146, 1999-2049, 10.1002/qj.3803, 2020.

Heslin-Rees, D., Burgos, M., Hansson, H. C., Krejci, R., Strom, J., Tunved, P., and Zieger, P.: From a polar to a marine environment: has the changing Arctic led to a shift in aerosol light scattering properties?, Atmospheric Chemistry and Physics, 20, 13671-13686, 10.5194/acp-20-13671-2020, 2020.

Hirdman, D., Sodemann, H., Eckhardt, S., Burkhart, J. F., Jefferson, A., Mefford, T., Quinn, P. K., Sharma, S., Strom, J., and Stohl, A.: Source identification of short-lived air pollutants in the Arctic using statistical analysis of measurement data and particle dispersion model output, Atmospheric Chemistry and Physics, 10, 669-693, 10.5194/acp-10-669-2010, 2010.

Hodshire, A. L., Campuzano-Jost, P., Kodros, J. K., Croft, B., Nault, B. A., Schroder, J. C., Jimenez, J. L., and Pierce, J. R.: The potential role of methanesulfonic acid (MSA) in aerosol formation and growth and the associated radiative forcings, Atmospheric Chemistry and Physics, 19, 3137-3160, 10.5194/acp-19-3137-2019, 2019.

Horn, S. J., Aasen, I. M., and Ostgaard, K.: Ethanol production from seaweed extract, Journal of Industrial Microbiology & Biotechnology, 25, 249-254, 10.1038/sj.jim.7000065, 2000.

Hu, Q. H., Xie, Z. Q., Wang, X. M., Kang, H., and Zhang, P. F.: Levoglucosan indicates high levels of biomass burning aerosols over oceans from the Arctic to Antarctic, Scientific Reports, 3, 7, 10.1038/srep03119, 2013.

Ion, A. C., Vermeylen, R., Kourtchev, I., Cafmeyer, J., Chi, X., Gelencser, A., Maenhaut, W., and Claeys, M.: Polar organic compounds in rural $PM_{2.5}$ aerosols from K-puszta, Hungary, during a 2003 summer field campaign: Sources and diel variations, Atmospheric Chemistry and Physics, 5, 1805-1814, 10.5194/acp-5-1805-2005, 2005.

Jacobsen, E. E., and Anthonsen, T.: 2-C-Methyl-D-erythritol. Produced in plants, forms aerosols in the atmosphere. An alternative pathway in isoprenoid biosynthesis, Biocatalysis and Biotransformation, 33, 191-196, 10.3109/10242422.2015.1095677, 2015.

Jiao, C. Y., and Flanner, M. G.: Changing black carbon transport to the Arctic from present day to the end of 21st century, Journal of Geophysical Research-Atmospheres, 121, 4734-4750, 10.1002/2015jd023964, 2016.

Jurányi, Z., Zanatta, M., Lund, M.T., Samset, B.H., Skeie, R.B., Sharma, S., Wendisch, M., Herber, A.: Atmospheric concentrations of black carbon are substantially higher in spring than summer in the Arctic. Communications Earth & Environment 4, 91, 2023. https://doi.org/10.1038/s43247-023-00749-x.

1180 Karlsen, S. R., Elvebakk, A., Hogda, K. A., and Grydeland, T.: Spatial and Temporal Variability in the
1181 Onset of the Growing Season on Svalbard, Arctic Norway - Measured by MODIS-NDVI Satellite Data,
1182 Remote Sensing, 6, 8088-8106, 10.3390/rs6098088, 2014.

1183 Klimont, Z., Kupiainen, K., Heyes, C., Purohit, P., Cofala, J., Rafaj, P., Borken-Kleefeld, J., and Schopp,
1184 W.: Global anthropogenic emissions of particulate matter including black carbon, Atmospheric
1185 Chemistry and Physics, 17, 8681-8723, 10.5194/acp-17-8681-2017, 2017.

1186 Kourtchev, I., Ruuskanen, T., Maenhaut, W., Kulmala, M., and Claeys, M.: Observation of 2-
1187 methyltetrols and related photo-oxidation products of isoprene in boreal forest aerosols from Hyytiala,
1188 Finland, Atmospheric Chemistry and Physics, 5, 2761-2770, 10.5194/acp-5-2761-2005, 2005.

1189 Kourtchev, I., Ruuskanen, T. M., Keronen, P., Sogacheva, L., Dal Maso, M., Reissell, A., Chi, X.,
1190 Vermeylen, R., Kulmala, M., Maenhaut, W., and Claeys, M.: Determination of isoprene and alpha-/beta-
1191 pinene oxidation products in boreal forest aerosols from Hyytiala, Finland: diel variations and possible
1192 link with particle formation events, Plant Biology, 10, 138-149, 10.1055/s-2007-964945, 2008a.

1193 Kourtchev, I., Warnke, J., Maenhaut, W., Hoffmann, T., and Claeys, M.: Polar organic marker
1194 compounds in $PM_{2.5}$ aerosol from a mixed forest site in western Germany, Chemosphere, 73, 1308-
1195 1314, 10.1016/j.chemosphere.2008.07.011, 2008b.

1196 Kramshoj, M., Vedel-Petersen, I., Schollert, M., Rinnan, A., Nymand, J., Ro-Poulsen, H., and Rinnan,
1197 R.: Large increases in Arctic biogenic volatile emissions are a direct effect of warming, Nature
1198 Geoscience, 9, 349-+, 10.1038/ngeo2692, 2016.

1199 Kunit, M., and Puxbaum, H.: Enzymatic determination of the cellulose content of atmospheric aerosols,
1200 Atmospheric Environment, 30, 1233-1236, 10.1016/1352-2310(95)00429-7, 1996.

1201 Li, S. M., Barrie, L. A., and Sirois, A.: Biogenic sulfur aerosol in the Arctic troposphere. 2. Trends and
1202 seasonal-variations, Journal of Geophysical Research-Atmospheres, 98, 20623-20631,
1203 10.1029/93jd02233, 1993.

1204 Liakakou, E., Vrekoussis, M., Bonsang, B., Donousis, C., Kanakidou, M., and Mihalopoulos, N.:
1205 Isoprene above the Eastern Mediterranean: Seasonal variation and contribution to the oxidation capacity
1206 of the atmosphere, Atmospheric Environment, 41, 1002-1010, 10.1016/j.atmosenv.2006.09.034, 2007.

1207 Lin, Y. H., Zhang, Z. F., Docherty, K. S., Zhang, H. F., Budisulistiorini, S. H., Rubitschun, C. L.,
1208 Shaw, S. L., Knipping, E. M., Edgerton, E. S., Kleindienst, T. E., Gold, A., and Surratt, J. D.: Isoprene
1209 Epoxydiols as Precursors to Secondary Organic Aerosol Formation: Acid-Catalyzed Reactive Uptake
1210 Studies with Authentic Compounds, Environmental Science & Technology, 46, 250-258,
1211 10.1021/es202554c, 2012.

1212 Long, C. M., Nascarella, M. A., and Valberg, P. A.: Carbon black vs. black carbon and other airborne
1213 materials containing elemental carbon: Physical and chemical distinctions, Environmental Pollution,
1214 181, 271-286, 10.1016/j.envpol.2013.06.009, 2013.

1215 Lopez-Hilfiker, F. D., Mohr, C., D'Ambro, E. L., Lutz, A., Riedel, T. P., Gaston, C. J., Iyer, S., Zhang,
1216 Z., Gold, A., Surratt, J. D., Lee, B. H., Kurten, T., Hu, W. W., Jimenez, J., Hallquist, M., and Thornton,
1217 J. A.: Molecular Composition and Volatility of Organic Aerosol in the Southeastern US: Implications
1218 for IEPDX Derived SOA, Environmental Science & Technology, 50, 2200-2209,
1219 10.1021/acs.est.5b04769, 2016.

1220 McCarty, J. L., Aalto, J., Paunu, V. V., Arnold, S. R., Eckhardt, S., Klimont, Z., Fain, J. J., Evangeliou,
1221 N., Venalainen, A., Tchebakova, N. M., Parfenova, E. I., Kupiainen, K., Soja, A. J., Huang, L., and

Wilson, S.: Reviews and syntheses: Arctic fire regimes and emissions in the 21st century, Biogeosciences, 18, 5053-5083, 10.5194/bg-18-5053-2021, 2021.

McDow, S. R., and Huntzicker, J. J.: Organic Aerosol Sampling Artifacts, Abstracts of Papers of the American Chemical Society, 200, 106-Envr, 1990.

Medeiros, P. M., Conte, M. H., Weber, J. C., and Simoneit, B. R. T.: Sugars as source indicators of biogenic organic carbon in aerosols collected above the Howland Experimental Forest, Maine, Atmospheric Environment, 40, 1694-1705, 10.1016/j.atmosenv.2005.11.001, 2006.

Moschos, V., Dzepina, K., Bhattu, D., Lamkaddam, H., Casotto, R., Daellenbach, K. R., Canonaco, F., Rai, P., Aas, W., Becagli, S., Calzolai, G., Eleftheriadis, K., Moffett, C. E., Schnelle-Kreis, J., Severi, M., Sharma, S., Skov, H., Vestenius, M., Zhang, W., Hakola, H., Hellén, H., Huang, L., Jaffrezo, J.-L., Massling, A., Nøjgaard, J. K., Petäjä, T., Popovicheva, O., Sheesley, R. J., Traversi, R., Yttri, K. E., Schmale, J., Prévôt, A. S. H., Baltensperger, U., and El Haddad, I.: Equal abundance of summertime natural and wintertime anthropogenic Arctic organic aerosols, Nature Geoscience, 10.1038/s41561-021-00891-1, 2022.

Myers-Smith, I. H., Kerby, J. T., Phoenix, G. K., Bjerke, J. W., Epstein, H. E., Assmann, J. J., John, C., Andreu-Hayles, L., Angers-Blondin, S., Beck, P. S. A., Berner, L. T., Bhatt, U. S., Bjorkman, A. D., Blok, D., Bryn, A., Christiansen, C. T., Cornelissen, J. H. C., Cunliffe, A. M., Elmendorf, S. C., Forbes, B. C., Goetz, S. J., Hollister, R. D., de Jong, R., Loranty, M. M., Macias-Fauria, M., Maseyk, K., Normand, S., Olofsson, J., Parker, T. C., Parmentier, F. J. W., Post, E., Schaepman-Strub, G., Stordal, F., Sullivan, P. F., Thomas, H. J. D., Tommervik, H., Treharne, R., Tweedie, C. E., Walker, D. A., Wilmking, M., and Wipf, S.: Complexity revealed in the greening of the Arctic, Nature Climate Change, 10, 106-117, 10.1038/s41558-019-0688-1, 2020.

Nolte, C. G., Schauer, J. J., Cass, G. R., and Simoneit, B. R. T.: Highly polar organic compounds present in wood smoke and in the ambient atmosphere, Environmental Science & Technology, 35, 1912-1919, 10.1021/es001420r, 2001.

Noziere, B., Gonzalez, N. J. D., Borg-Karlson, A. K., Pei, Y. X., Redeby, J. P., Krejci, R., Dommen, J., Prevot, A. S. H., and Anthonsen, T.: Atmospheric chemistry in stereo: A new look at secondary organic aerosols from isoprene, Geophysical Research Letters, 38, 10.1029/2011gl047323, 2011.

Noziere, B., Kalberer, M., Claeys, M., Allan, J., D'Anna, B., Decesari, S., Finessi, E., Glasius, M., Grgic, I., Hamilton, J. F., Hoffmann, T., Iinuma, Y., Jaoui, M., Kahno, A., Kampf, C. J., Kourtchev, I., Maenhaut, W., Marsden, N., Saarikoski, S., Schnelle-Kreis, J., Surratt, J. D., Szidat, S., Szmigielski, R., and Wisthaler, A.: The Molecular Identification of Organic Compounds in the Atmosphere: State of the Art and Challenges, Chemical Reviews, 115, 3919-3983, 10.1021/cr5003485, 2015a.

Ottar, B.: Arctic air-pollution - A Norwegian Perspective, Atmospheric Environment, 23, 2349-2356, 10.1016/0004-6981(89)90248-5, 1989.

Paasonen, P., Asmi, A., Petaja, T., Kajos, M. K., Aijala, M., Junninen, H., Holst, T., Abbatt, J. P. D., Arneth, A., Birmili, W., van der Gon, H. D., Hamed, A., Hoffer, A., Laakso, L., Laaksonen, A., Leaitch,

Paulot, F., Crounse, J. D., Kjaergaard, H. G., Kurten, A., St Clair, J. M., Seinfeld, J. H., and Wennberg, P. O.: Unexpected Epoxide Formation in the Gas-Phase Photooxidation of Isoprene, Science, 325, 730-733, 10.1126/science.1172910, 2009.

Pisso, I., Sollum, E., Grythe, H., Kristiansen, N. I., Cassiani, M., Eckhardt, S., Arnold, D., Morton, D., Thompson, R. L., Zwaaftink, C. D. G., Evangeliou, N., Sodemann, H., Haimberger, L., Henne, S., Brunner, D., Burkhart, J. F., Fouilloux, A., Brioude, J., Philipp, A., Seibert, P., and Stohl, A.: The

Lagrangian particle dispersion model FLEXPART version 10.4, Geoscientific Model Development, 12, 4955-4997, 10.5194/gmd-12-4955-2019, 2019.

Platt, S. M., Hov, O., Berg, T., Breivik, K., Eckhardt, S., Eleftheriadis, K., Evangeliou, N., Fiebig, M., Fisher, R., Hansen, G., Hansson, H. C., Heintzenberg, J., Hermansen, O., Heslin-Rees, D., Holmen, K., Hudson, S., Kallenborn, R., Krejci, R., Krognes, T., Larssen, S., Lowry, D., Myhre, C. L., Lunder, C., Nisbet, E., Nizzetto, P. B., Park, K. T., Pedersen, C. A., Pfaffhuber, K. A., Rockmann, T., Schmidbauer, N., Solberg, S., Stohl, A., Strom, J., Svendby, T., Tunved, P., Tornkvist, K., van der Veen, C., Vratolis, S., Yoon, Y. J., Yttri, K. E., Zieger, P., Aas, W., and Torseth, K.: Atmospheric composition in the European Arctic and 30 years of the Zeppelin Observatory, Ny-Ålesund, Atmospheric Chemistry and Physics, 22, 3321-3369, 10.5194/acp-22-3321-2022, 2022.

Platt, S. M., et al.: Source apportionment of equivalent black carbon from the winter 2017–2018 EMEP intensive measurement campaign using PMF, in preparation, 2023.

Prospero, J. M., Blades, E., Mathison, G., and Naidu, R.: Interhemispheric transport of viable fungi and bacteria from Africa to the Caribbean with soil dust, Aerobiologia, 21, 1-19, 10.1007/s10453-004-5872-7, 2005.

Pueschel, R. F., and Kinne, S. A.: Physical and radiative properties of Arctic atmospheric aerosols, Science of the Total Environment, 160-61, 811-824, 10.1016/0048-9697(95)04414-v, 1995.

Puxbaum, H., and Tenze-Kunit, M.: Size distribution and seasonal variation of atmospheric cellulose, Atmospheric Environment, 37, 3693-3699, 10.1016/s1352-2310(03)00451-5, 2003.

Qi, L., Vogel, A. L., Esmaeilirad, S., Cao, L. M., Zheng, J., Jaffrezo, J. L., Fermo, P., Kasper-Giebl, A., Daellenbach, K. R., Chen, M. D., Ge, X. L., Baltensperger, U., Prevot, A. S. H., and Slowik, J. G.: A 1-year characterization of organic aerosol composition and sources using an extractive electrospray ionization time-of-flight mass spectrometer (EESI-TOF), Atmospheric Chemistry and Physics, 20, 7875-7893, 10.5194/acp-20-7875-2020, 2020.

Quinn, P. K., Miller, T. L., Bates, T. S., Ogren, J. A., Andrews, E., and Shaw, G. E.: A 3-year record of simultaneously measured aerosol chemical and optical properties at Barrow, Alaska, Journal of Geophysical Research-Atmospheres, 107, 10.1029/2001jd001248, 2002.

Quinn, P. K., Shaw, G., Andrews, E., Dutton, E. G., Ruoho-Airola, T., and Gong, S. L.: Arctic haze: current trends and knowledge gaps, Tellus Series B-Chemical and Physical Meteorology, 59, 99-114, 10.1111/j.1600-0889.2006.00238.x, 2007.

Quinn, P. K., Bates, T. S., Schulz, K., and Shaw, G. E.: Decadal trends in aerosol chemical composition at Barrow, Alaska: 1976-2008, Atmospheric Chemistry and Physics, 9, 8883-8888, 10.5194/acp-9-8883-2009, 2009.

Rauber, M., Salazar, G., Yttri, K. E., and Szidat, S.: An optimised organic carbon/elemental carbon (OC/EC) fraction separation method for radiocarbon source apportionment applied to low-loaded Arctic aerosol filters, Atmos. Meas. Tech., 16, 825–844, https://doi.org/10.5194/amt-16-825-2023, 2023.

Rauber, M. et al.: Organic aerosols at Trollhaugen Observatory (Antarctica) in summer are dominated by marine sources. In preparation, 2023.

Ricard, V., Jaffrezo, J. L., Kerminen, V. M., Hillamo, R. E., Sillanpaa, M., Ruellan, S., Liousse, C., and Cachier, H.: Two years of continuous aerosol measurements in northern Finland, Journal of Geophysical Research-Atmospheres, 107, 10.1029/2001jd000952, 2002.

Riipinen, I., Pierce, J. R., Yli-Juuti, T., Nieminen, T., Hakkinen, S., Ehn, M., Junninen, H., Lehtipalo, K., Petaja, T., Slowik, J., Chang, R., Shantz, N. C., Abbatt, J., Leaitch, W. R., Kerminen, V. M., Worsnop, D. R., Pandis, S. N., Donahue, N. M., and Kulmala, M.: Organic condensation: a vital link connecting aerosol formation to cloud condensation nuclei (CCN) concentrations, Atmospheric Chemistry and Physics, 11, 3865-3878, 10.5194/acp-11-3865-2011, 2011.

Rotzer, T., and Chmielewski, F. M.: Phenological maps of Europe, Climate Research, 18, 249-257, 10.3354/cr018249, 2001.

Sagner, S., Eisenreich, W., Fellermeier, M., Latzel, C., Bacher, A., and Zenk, M. H.: Biosynthesis of 2-C-methyl-D-erythritol in plants by rearrangement of the terpenoid precursor, 1-deoxy-D-xylulose 5-phosphate, Tetrahedron Letters, 39, 2091-2094, 10.1016/s0040-4039(98)00296-2, 1998.

Samake, A., Jaffrezo, J. L., Favez, O., Weber, S., Jacob, V., Canete, T., Albinet, A., Charron, A., Riffault, V., Perdrix, E., Waked, A., Golly, B., Salameh, D., Chevrier, F., Oliveira, D. M., Besombes, J. L., Martins, J. M. F., Bonnaire, N., Conil, S., Guillaud, G., Mesbah, B., Rocq, B., Robic, P. Y., Hulin, A., Le Meur, S., Descheemaecker, M., Chretien, E., Marchand, N., and Uzu, G.: Arabitol, mannitol, and glucose as tracers of primary biogenic organic aerosol: the influence of environmental factors on ambient air concentrations and spatial distribution over France, Atmospheric Chemistry and Physics, 19, 11013-11030, 10.5194/acp-19-11013-2019, 2019.

Samake, A., Bonin, A., Jaffrezo, J. L., Taberlet, P., Weber, S., Uzu, G., Jacob, V., Conil, S., and Martins, J. M. F.: High levels of primary biogenic organic aerosols are driven by only a few plant-associated microbial taxa, Atmospheric Chemistry and Physics, 20, 5609-5628, 10.5194/acp-20-5609-2020, 2020.

Sanchez-Ochoa, A., Kasper-Giebl, A., Puxbaum, H., Gelencser, A., Legrand, M., and Pio, C.: Concentration of atmospheric cellulose: A proxy for plant debris across a west-east transect over Europe, Journal of Geophysical Research-Atmospheres, 112, 10.1029/2006jd008180, 2007.

Sandradewi, J., Prevot, A. S. H., Szidat, S., Perron, N., Alfarra, M. R., Lanz, V. A., Weingartner, E., and Baltensperger, U.: Using aerosol light absorption measurements for the quantitative determination of wood burning and traffic emission contributions to particulate matter, Environmental Science & Technology, 42, 3316-3323, 10.1021/es702253m, 2008.

Schmale, J., Zieger, P., and Ekman, A. M. L.: Aerosols in current and future Arctic climate, Nature Climate Change, 11, 95-105, 10.1038/s41558-020-00969-5, 2021.

Schmidl, C., Marr, L. L., Caseiro, A., Kotianova, P., Berner, A., Bauer, H., Kasper-Giebl, A., and Puxbaum, H.: Chemical characterisation of fine particle emissions from wood stove combustion of common woods growing in mid-European Alpine regions, Atmospheric Environment, 42, 126-141, 10.1016/j.atmosenv.2007.09.028, 2008.

Serreze, M. C., and Barry, R. G.: Processes and impacts of Arctic amplification: A research synthesis, Global and Planetary Change, 77, 85-96, 10.1016/j.gloplacha.2011.03.004, 2011.

Sharma, S., Chan, E., Ishizawa, M., Toom-Sauntry, D., Gong, S. L., Li, S. M., Tarasick, D. W., Leaitch, W. R., Norman, A., Quinn, P. K., Bates, T. S., Levasseur, M., Barrie, L. A., and Maenhaut, W.: Influence of transport and ocean ice extent on biogenic aerosol sulfur in the Arctic atmosphere, Journal of Geophysical Research-Atmospheres, 117, 10.1029/2011jd017074, 2012.

Sharma, S., Barrie, L. A., Magnusson, E., Brattstrom, G., Leaitch, W. R., Steffen, A., and Landsberger, S.: A Factor and Trends Analysis of Multidecadal Lower Tropospheric Observations of Arctic Aerosol Composition, Black Carbon, Ozone, and Mercury at Alert, Canada, Journal of Geophysical Research-Atmospheres, 124, 14133-14161, 10.1029/2019jd030844, 2019.

1351 Shaw, G. E.: The arctic haze phenomenon, Bulletin of the American Meteorological Society, 76, 2403-
1352 2413, 10.1175/1520-0477(1995)076<2403:tahp>2.0.co;2, 1995.

1353 Simoneit, B. R. T., Schauer, J. J., Nolte, C. G., Oros, D. R., Elias, V. O., Fraser, M. P., Rogge, W. F.,
1354 and Cass, G. R.: Levoglucosan, a tracer for cellulose in biomass burning and atmospheric particles,
1355 Atmospheric Environment, 33, 173-182, 10.1016/s1352-2310(98)00145-9, 1999.

1356 Simpson, D., Yttri, K. E., Klimont, Z., Kupiainen, K., Caseiro, A., Gelencser, A., Pio, C., Puxbaum, H.,
1357 and Legrand, M.: Modeling carbonaceous aerosol over Europe: Analysis of the CARBOSOL and EMEP
1358 EC/OC campaigns, Journal of Geophysical Research-Atmospheres, 112, 10.1029/2006JD008158, 2007.

1359 Solomon, A., de Boer, G., Creamean, J. M., McComiskey, A., Shupe, M. D., Maahn, M., and Cox, C.:
1360 The relative impact of cloud condensation nuclei and ice nucleating particle concentrations on phase
1361 partitioning in Arctic mixed-phase stratocumulus clouds, Atmospheric Chemistry and Physics, 18,
1362 17047-17059, 10.5194/acp-18-17047-2018, 2018.

1363 Stohl, A., Forster, C., Frank, A., Seibert, P., and Wotawa, G.: Technical note: The Lagrangian particle
1364 dispersion model FLEXPART version 6.2, Atmospheric Chemistry and Physics, 5, 2461-2474,
1365 10.5194/acp-5-2461-2005, 2005.

1366 Stohl, A., Andrews, E., Burkhart, J. F., Forster, C., Herber, A., Hoch, S. W., Kowal, D., Lunder, C.,
1367 Mefford, T., Ogren, J. A., Sharma, S., Spichtinger, N., Stebel, K., Stone, R., Strom, J., Torseth, K.,
1368 Wehrli, C., and Yttri, K. E.: Pan-Arctic enhancements of light absorbing aerosol concentrations due to
1369 North American boreal forest fires during summer 2004, Journal of Geophysical Research-
1370 Atmospheres, 111, 10.1029/2006JD007216, 2006.

1371 Stohl, A., Berg, T., Burkhart, J. F., Fjaeraa, A. M., Forster, C., Herber, A., Hov, O., Lunder, C.,
1372 McMillan, W. W., Oltmans, S., Shiobara, M., Simpson, D., Solberg, S., Stebel, K., Strom, J., Torseth,
1373 K., Treffeisen, R., Virkkunen, K., and Yttri, K. E.: Arctic smoke - record high air pollution levels in the
1374 European Arctic due to agricultural fires in Eastern Europe in spring 2006, Atmospheric Chemistry and
1375 Physics, 7, 511-534, 2007.

1376 Stohl, A., Klimont, Z., Eckhardt, S., Kupiainen, K., Shevchenko, V. P., Kopeikin, V. M., and
1377 Novigatsky, A. N.: Black carbon in the Arctic: the underestimated role of gas flaring and residential
1378 combustion emissions, Atmospheric Chemistry and Physics, 13, 8833-8855, 10.5194/acp-13-8833-
1379 2013, 2013.

1380 Surratt, J. D., Chan, A. W. H., Eddingsaas, N. C., Chan, M. N., Loza, C. L., Kwan, A. J., Hersey, S. P.,
1381 Flagan, R. C., Wennberg, P. O., and Seinfeld, J. H.: Reactive intermediates revealed in secondary
1382 organic aerosol formation from isoprene, Proceedings of the National Academy of Sciences of the
1383 United States of America, 107, 6640-6645, 10.1073/pnas.0911114107, 2010.

1384 Tobo, Y., Adachi, K., DeMott, P. J., Hill, T. C. J., Hamilton, D. S., Mahowald, N. M., Nagatsuka, N.,
1385 Ohata, S., Uetake, J., Kondo, Y., and Koike, M.: Glacially sourced dust as a potentially significant
1386 source of ice nucleating particles, Nature Geoscience, 12, 253-+, 10.1038/s41561-019-0314-x, 2019.

1387 Tobler, A. K., Skiba, A., Canonaco, F., Mocnik, G., Rai, P., Chen, G., Bartyzel, J., Zimnoch, M.,
1388 Styszko, K., Necki, J., Furger, M., Rózanski, K., Baltensperger, U., Slowik, J. G., and Prevot, A. S. H.:
1389 Characterization of non-refractory (NR) PM_1 and source apportionment of organic aerosol in Krakow,
1390 Poland, Atmospheric Chemistry and Physics, 21, 14893-14906, 10.5194/acp-21-14893-2021, 2021.

1391 Tonon, T., Li, Y., and McQueen-Mason, S.: Mannitol biosynthesis in algae: more widespread and
1392 diverse than previously thought, New Phytologist, 213, 1573-1579, 10.1111/nph.14358, 2017.

Turpin, B. J., and Lim, H. J.: Species contributions to $PM_{2.5}$ mass concentrations: Revisiting common assumptions for estimating organic mass, Aerosol Science and Technology, 35, 602-610, 10.1080/02786820119445, 2001.

Tørseth, K., Andrews, E., Asmi, E., Eleftheriadis, K., Fiebig, M., Herber, A., Huang, L., Kylling, A, Lupi, A., Massling, A., Mazzola, M. Klenø Nøjgaard, J., Popovicheva, O., Schichtel, B., Schmale, J., Sharma, S: Review of observation capacities and data availability for Black Carbon in the Arctic region - Technical Report 1. December 2019. iv + 35pp.

van der Werf, G. R., Randerson, J. T., Giglio, L., van Leeuwen, T. T., Chen, Y., Rogers, B. M., Mu, M. Q., van Marle, M. J. E., Morton, D. C., Collatz, G. J., Yokelson, R. J., and Kasibhatla, P. S.: Global fire emissions estimates during 1997-2016, Earth System Science Data, 9, 697-720, 10.5194/essd-9-697-2017, 2017.

Vegetation in Svalbard: https://www.npolar.no/en/themes/vegetation-svalbard/, last access: 9 February 2023.

von Schneidemesser, E., Schauer, J. J., Hagler, G. S. W., and Bergin, M. H.: Concentrations and sources of carbonaceous aerosol in the atmosphere of Summit, Greenland, Atmospheric Environment, 43, 4155-4162, 10.1016/j.atmosenv.2009.05.043, 2009.

Waked, A., Favez, O., Alleman, L. Y., Piot, C., Petit, J. E., Delaunay, T., Verlinden, E., Golly, B., Besombes, J. L., Jaffrezo, J. L., and Leoz-Garziandia, E.: Source apportionment of PM10 in a north-western Europe regional urban background site (Lens, France) using positive matrix factorization and including primary biogenic emissions, Atmospheric Chemistry and Physics, 14, 3325-3346, 10.5194/acp-14-3325-2014, 2014.

Wennberg, P. O., Bates, K. H., Crounse, J. D., Dodson, L. G., McVay, R. C., Mertens, L. A., Nguyen, T. B., Praske, E., Schwantes, R. H., Smarte, M. D., St Clair, J. M., Teng, A. P., Zhang, X., and Seinfeld, J. H.: Gas-Phase Reactions of Isoprene and Its Major Oxidation Products, Chemical Reviews, 118, 3337-3390, 10.1021/acs.chemrev.7b00439, 2018.

Winiger, P., Andersson, A., Yttri, K. E., Tunved, P., and Gustafsson, O.: Isotope-Based Source Apportionment of EC Aerosol Particles during Winter High-Pollution Events at the Zeppelin Observatory, Svalbard, Environmental Science & Technology, 49, 11959-11966, 10.1021/acs.est.5b02644, 2015.

Williams, J. and Koppmann, R.J. (2007) Volatile organic compounds in the atmosphere: An overview. In: Volatile organic compounds in the atmosphere. Ed. by: R. Koppmann. Oxford, Blackwell Publishing. pp. 1-19.

Winiger, P., Barrett, T. E., Sheesley, R. J., Huang, L., Sharma, S., Barrie, L. A., Yttri, K. E., Evangeliou, N., Eckhardt, S., Stohl, A., Klimont, Z., Heyes, C., Semiletov, I. P., Dudarev, O. V., Charkin, A., Shakhova, N., Holmstrand, H., Andersson, A., and Gustafsson, O.: Source apportionment of circum-Arctic atmospheric black carbon from isotopes and modeling, Science Advances, 5, 10.1126/sciadv.aau8052, 2019.

Xia, X., and Hopke, P. K.: Seasonal variation of 2-methyltetrols in ambient air samples, Environmental Science & Technology, 40, 6934-6937, 10.1021/es060988l, 2006.

Yttri, K. E., Aas, W., Bjerke, A., Cape, J. N., Cavalli, F., Ceburnis, D., Dye, C., Emblico, L., Facchini, M. C., Forster, C., Hanssen, J. E., Hansson, H. C., Jennings, S. G., Maenhaut, W., Putaud, J. P., and Torseth, K.: Elemental and organic carbon in PM_{10}: a one year measurement campaign within the

European Monitoring and Evaluation Programme EMEP, Atmospheric Chemistry and Physics, 7, 5711-5725, 2007b.

Yttri, K. E., Dye, C., and Kiss, G.: Ambient aerosol concentrations of sugars and sugar-alcohols at four different sites in Norway, Atmospheric Chemistry and Physics, 7, 4267-4279, 2007a.

Yttri, K. E., Simpson, D., Nojgaard, J. K., Kristensen, K., Genberg, J., Stenstrom, K., Swietlicki, E., Hillamo, R., Aurela, M., Bauer, H., Offenberg, J. H., Jaoui, M., Dye, C., Eckhardt, S., Burkhart, J. F., Stohl, A., and Glasius, M.: Source apportionment of the summer time carbonaceous aerosol at Nordic rural background sites, Atmospheric Chemistry and Physics, 11, 13339-13357, 10.5194/acp-11-13339-2011, 2011b.

Yttri, K. E., Simpson, D., Stenstrom, K., Puxbaum, H., and Svendby, T.: Source apportionment of the carbonaceous aerosol in Norway - quantitative estimates based on C-14, thermal-optical and organic tracer analysis, Atmospheric Chemistry and Physics, 11, 9375-9394, 10.5194/acp-11-9375-2011, 2011a.

Yttri, K. E., Myhre, C. L., Eckhardt, S., Fiebig, M., Dye, C., Hirdman, D., Stroem, J., Klimont, Z., and Stohl, A.: Quantifying black carbon from biomass burning by means of levoglucosan - a one-year time series at the Arctic observatory Zeppelin, Atmospheric Chemistry and Physics, 14, 6427-6442, 10.5194/acp-14-6427-2014, 2014.

Yttri, K. E., Canonaco, F., Eckhardt, S., Evangeliou, N., Fiebig, M., Gundersen, H., Hjellbrekke, A. G., Myhre, C. L., Platt, S. M., Prevot, A. S. H., Simpson, D., Solberg, S., Surratt, J., Torseth, K., Uggerud, H., Vadset, M., Wan, X., and Aas, W.: Trends, composition, and sources of carbonaceous aerosol at the Birkenes Observatory, northern Europe, 2001-2018, Atmospheric Chemistry and Physics, 21, 7149-7170, 10.5194/acp-21-7149-2021, 2021.

Zangrando, R., Barbaro, E., Zennaro, P., Rossi, S., Kehrwald, N. M., Gabrieli, J., Barbante, C., and Gambaro, A.: Molecular Markers of Biomass Burning in Arctic Aerosols, Environmental Science & Technology, 47, 8565-8574, 10.1021/es400125r, 2013.

Zieger, P., Heslin-Rees, D., Karlsson, L., Koike, M., Modini, R., and Krejci, R.: Black carbon scavenging by low-level Arctic clouds, Nature Communications, 14, 10.1038/s41467-023-41221-w, 2023.

Zwaaftink, C. D. G., Grythe, H., Skov, H., and Stohl, A.: Substantial contribution of northern high-latitude sources to mineral dust in the Arctic, Journal of Geophysical Research-Atmospheres, 121, 13678-13697, 10.1002/2016jd025482, 2016.

Zwaaftink, C. D. G., Aas, W., Eckhardt, S., Evangeliou, N., Hamer, P., Johnsrud, M., Kylling, A., Platt, S. M., Stebel, K., Uggerud, H., and Yttri, K. E.: What caused a record high PM10 episode in northern Europe in October 2020?, Atmospheric Chemistry and Physics, 22, 3789-3810, 10.5194/acp-22-3789-2022, 2022.

Table 1: Annual and seasonal mean concentrations of OC, OC_B (OC on backup filters) EC, TC, and organic tracers at Zeppelin Observatory, 2017 to 2020.

	OC (ng C m^{-3})	**OC_B** (ng C m^{-3})	**EC** (ng C m^{-3})	**TC** (ng C m^{-3})	**Cellul.** (ng m^{-3})	**Levogl.** (pg m^{-3})	**Mannos.** (pg m^{-3})	**Galactos.** (pg m^{-3})	**Arabitol** (pg m^{-3})	**Mannitol** (pg m^{-3})	**Fructose** (pg m^{-3})	**Glucose** (pg m^{-3})	**Trehalose** (pg m^{-3})	**2-methylery.** (pg m^{-3})	**2-methylthr.** (pg m^{-3})
2017	**121**	**32.9**	**11.6**	**132**	**2.1**	**465**	**53.5**	**18.7**	**99.7**	**115**	**80.9**	**250**	**140**	**99.2**	**43.7**
DJF	99.6		14.8	116	2.1	862	120	38.1	29.5	29.7	130	106	31.7	5.6	3.5
MAM	128		20.8	149	2.1	83.4	11.9	3.5	7.7	15.1	32.4	123	64.0	6.1	3.8
JJA	94.5		3.5	97.6	1.6	160	33.2	10.8	70.2	93.1	58.6	189	154	205	87.6
SON	146		9.7	156	2.4	725	59.4	23.8	235	260	1051	484	251	134	59.7
2018	**90.3**	**22.0**	**6.5**	**96.1**	**1.2**	**335**	**62.7**	**22.4**	**59.1**	**69.4**	**63.9**	**269**	**71.8**	**80.9**	**43.1**
DJF	88.5		9.7	98.1	1.3	587	66.3	22.6	38.6	49.7	105	137	37.6	4.8	2.8
MAM	101		11.3	112	1.3	150	15.0	8.0	11.8	15.3	55.5	183	43.9	13.2	8.4
JJA	123		4.5	127	1.4	481	113	42.4	137	156	84.1	494	144	217	113
SON	48.3		3.0	50.3	0.9	236	52.7	14.8	31.7	38.9	32.2	176	39.2	38.4	21.8
2019	**102**	**24.2**	**12.5**	**115**	**1.3**	**547**	**120**	**30.2**	**138**	**161**	**90.7**	**504**	**217**	**251**	**113**
DJF	109		24.2	133	1.3	1124	152	38.6	27.0	18.4	62.0	583	47.4	7.1	5.5
MAM	79.0		15.1	94.1	1.2	127	19.8	5.6	10.7	17.0	49.2	209	135	6.5	4.0
JJA	169		9.2	178	1.6	530	181	47.8	265	306	107	707	250	812	366
SON	63.1		3.6	66.5	1.0	565	148	34.8	251	301	144	581	410	212	93.1
2020	**197**	**32.6**	**16.3**	**214**	**1.6**	**919**	**175**	**54.7**	**242**	**172**	**179**	**808**	**188**	**644**	**502**
DJF	85.9		14.5	101	1.5	1370	205	69.6	29.0	25.6	75.7	431	64.6	7.4	4.5
MAM	137		25.2	163	1.2	229	29.3	12.3	22.5	22.7	24.3	145	36.3	15.5	8.8
JJA	334		10.8	345	1.9	1292	299	86.2	659	415	473	2160	386	2350	1850
SON	202		13.7	216	2.1	963	188	58.8	226	207	129	424	260	47.5	24.0
Mean ±SD															
Annual	**128±48.0**	**27.9±5.6**	**11.7±4.0**	**139±51.7**	**1.6±0.2**	**567±251**	**103±56.2**	**31.5±16.2**	**135±78.5**	**129±46.8**	**104±51.5**	**457±260**	**154±63.6**	**267±261**	**176±220**
DJF	95.8±11.0		15.8±6.1	112±16.2	1.5±0.4	986±337	136±58.0	42.2±19.7	31.0±5.2	30.9±13.4	93.0±30.2	314±213	45.3±14.4	6.2±1.2	4.1±1.2
MAM	111±26.1		18.1±6.1	129±31.8	1.4±0.4	147±61.0	19.0±7.6	7.4±3.8	13.2±6.5	17.±3.6.	40.4±14.5	168±38.5	69.9±45.1	10.3±4.7	6.3±2.7
JJA	180±107		7.0±3.5	187±110	1.6±0.1	616±480	157±113	46.8±30.9	283±264	243±146	181±196	888±876	234±113	896±1010	604±839
SON	115±72.3		7.5±5.1	122±77.8	1.6±0.7	622±305	112±66.6	33.1±19.0	186±103	202±115	103±49.4	416±173	240±152	108±81.4	49.7±33.8
H-S	102±19.0		15.7±4.1	117±23.0	1.5±0.4	518±156	68.9±24.7	22.8±9.4	23.7±3.6	26.1±2.0	77.3±21.8	233±105	79±63	9.2±3.0	5.7±1.7
NH-S	152±75.0		7.6±3.3	163±86.0	1.7±0.5	622±374	152±111	41.4±25.3	258±160	246±108	148±115	703±472	235±96	555±530	360±445

Notations: H-S = Heating season (November to May); NH-S = Non-heating season (June - October)

Table 2: Estimated annual mean concentrations (eq. 1 – 7) of sea salt aerosol (SSA), mineral dust (MD), non-sea salt sulfate (nss-SO_4^{2-}), organic matter (OM = OC × 2.2; Turpin and Lim, 2001), and elemental carbon (EC) at Zeppelin Observatory 2017 to 2020. Unit: ng m^{-3}.

	SSA	**MD[1)]**	**nss-SO_4^{2-}**	**OM**	**EC**
2017	730	559	381	265	11.6
2018	618	279	243	199	6.5
2019	697	477	283	225	12.5
2020	684	1136	349	434	16.3
Mean ± SD	682 ± 46.9	613 ± 368	314 ± 62.6	281 ± 106	12 4.0

1) 3 µm EAD size fraction (10 µm EAD for other variables).

Table 3: Annual, heating season, and non-heating season contributions of BB and FF to eBC (PMF) and BC (FLEXPART). BB is denoted RWC in the heating season and WF in the non-heating season. Heating season and non-heating season contributions of levoglucosan are included. Zeppelin Observatory, 2017 to 2020. Unit: %.

	2017		**2018**		**2019**		**2020**		**Mean ± SD**	**Mean ± SD**
	PMF	**FLEXPART**	**PMF**	**FLEXPART**	**PMF**	**FLEXPART**	**PMF**	**FLEXPART**	**PMF**	**FLEXPART**
Annual										
eBC_{FF}/eBC	71	54	68	47	73	53	67	*50*	*70 ± 2.7*	*51 ± 3.1*
eBC_{BB}/eBC	29	46	32	53	27	47	33	*50*	*30 ± 2.7*	*49 ± 3.1*
Heating season										
eBC_{FF}/eBC	73	59	67	51	73	58	70	*57*	*71 ± 2.7*	*56 ± 3.6*
eBC_{RWC}/eBC	27	41	33	49	27	42	30	*43*	*29 ± 2.7*	*44 ± 3.6*
Non-heating season										
eBC_{FF}/eBC	65	43	72	35	73	41	58	*37*	*67 ± 6.7*	*39 ± 3.3*
eBC_{WF}/eBC	35	57	28	65	27	59	42	*63*	*33 ± 6.7*	*61 ± 3.3*
Seasonal/Annual										
$eBC_{FF\_H\text{-}S}/eBC_{FF}$	77	73	80	80	78	79	75	*74*	*77 ± 1.8*	*77 ± 3.8*
$eBC_{FF\_NH\text{-}S}/eBC_{FF}$	23	27	20	20	22	21	25	*26*	*23 ± 1.8*	*23 ± 3.8*
eBC_{RWC}/eBC_{BB}	69	58	83	68	78	65	65	*55*	*74 ± 8.2*	*62 ± 6.0*
eBC_{WF}/eBC_{BB}	31	42	17	32	22	35	35	*45*	*26 ± 8.2*	*38 ± 6.0*
Seasonal/Annual										
$eBC_{FF\_H\text{-}S}/eBC$	55	39	54	38	56	42	50	37	*54 ± 2.8*	*39 ± 2.4*
$eBC_{FF\_NH\text{-}S}/eBC$	16	14	14	9	16	11	17	13	*16 ± 1.2*	*12 ± 2.3*
eBC_{RWC}/eBC	20	27	26	36	21	31	22	28	*22 ± 2.7*	*30 ± 4.1*
eBC_{WF}/eBC	8.9	20	5.4	17	6.1	16	12	22	*8.0 ± 2.9*	*19 ± 2.8*

Notation: eBC = equivalent black carbon; FF = fossil fuel; BB = biomass burning; H-S = Heating season; NH-S = Non-heating season; Levo = Levoglucosan; WF = Wildfire; RWC = Residential wood combustion; For simplicity we state eBC for both PMF and FLEXPART methods, while the correct is BC for FLEXPART.

Table 4: BB and FF fractions of BC (monthly weighted) obtained by different approaches (PMF, FLEXPART, and Radiocarbon;LHS) for non-heating-season and heating season. Means are based on identical time periods (See Table S3).

Methodology	Annual		NH-season (JJASO)		H-season (NDJFMAM)	
	BC_{BB}/BC	BC_{FF}/BC	BC_{BB}/BC	BC_{FF}/BC	BC_{BB}/BC	BC_{FF}/BC
PMF	27 ± 14	73 ± 14	31 ± 11	69 ± 11	25 ± 16	75 ± 16
FLEXPART	45 ± 5	55 ± 5	48 ± 18	52 ± 18	42 ± 10	58 ± 10
Radiocarbon;LHS	61 ± 15	39 ± 15	67 ± 5	33 ± 5	57 ± 18	43 ± 18

Notation: For simplicity we state BC for all methods, while the correct is eBC for PMF, BC for FLEXPART, and EC for Radiocarbon;LHS.

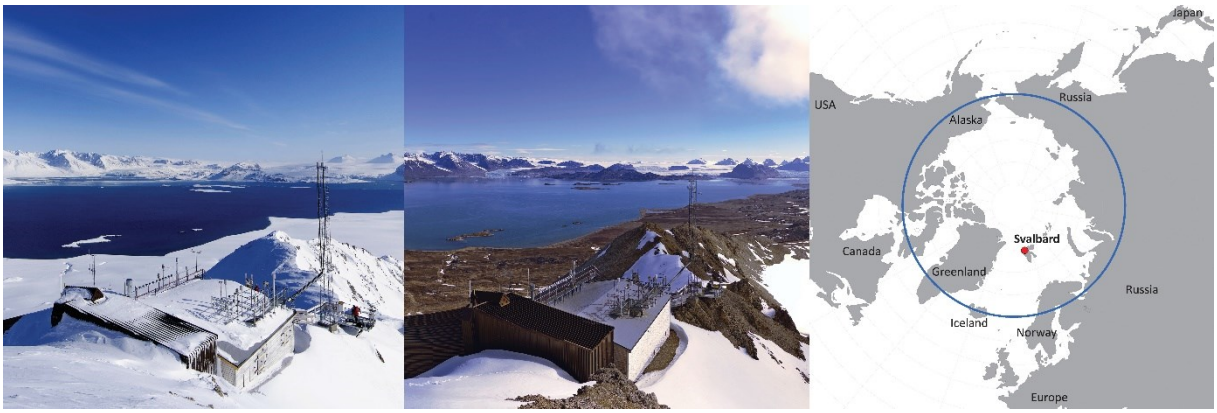

Figure 1. The Zeppelin observatory located at the Zeppelin Mountain (472 m a.s.l.) close to the Ny-Ålesund settlement at Svalbard (78˚54´0 N, 11˚53´0 E) in: winter (left panel); summer (middle panel); The light-blue line on the map shows the Arctic Circle (66 ˚North) (right panel). (Foto: Ove Hermansen, NILU; Map: Finn Bjørklid, NILU).

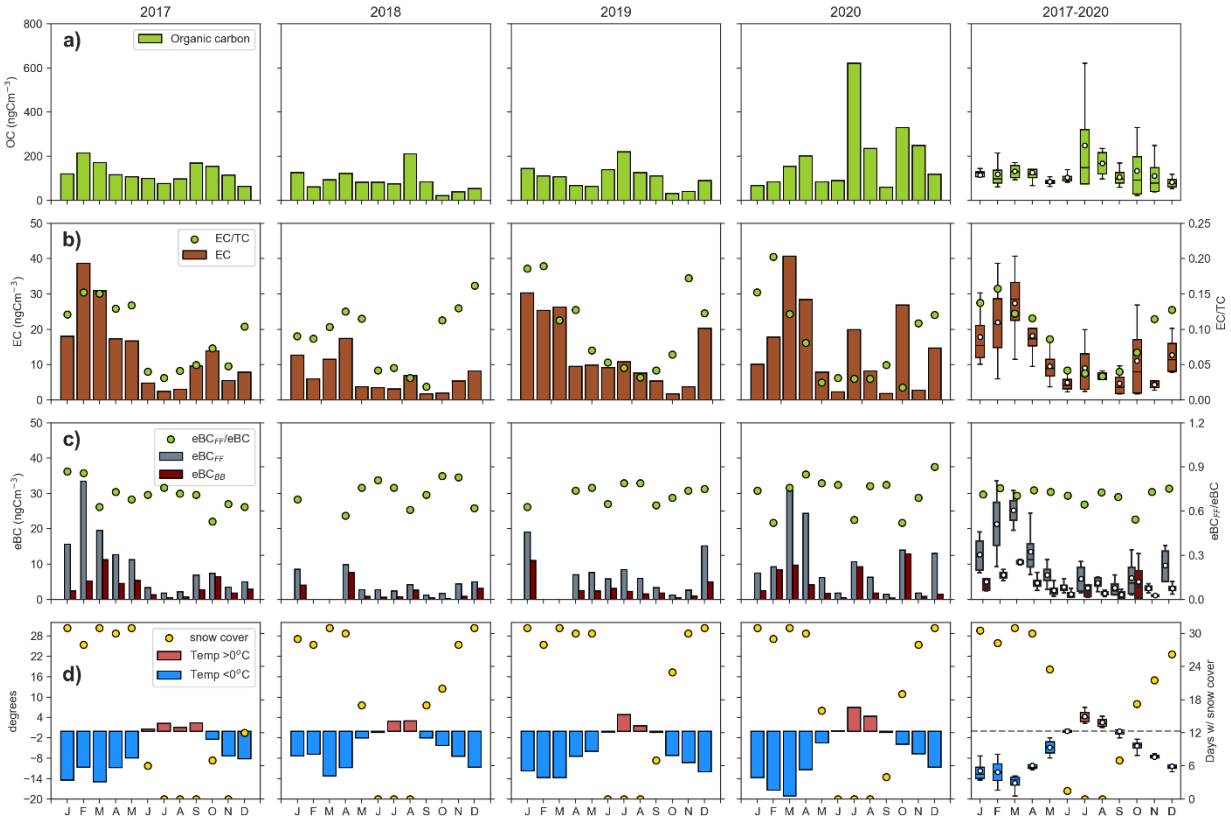

Figure 2. Panels show monthly mean concentrations for 2017 to 2020 and box plots (mean, 25, 50, 75 percentiles and IQR) for 2017 to 2020 at Zeppelin Observatory for a) OC; b) EC and EC/TC; c) eBC_{BB}, eBC_{FF}, and eBC_{FF}/eBC; d) Ambient temperature and days with snow on ground. Concentrations in a) - c) are measured in the PM_{10} size fraction.

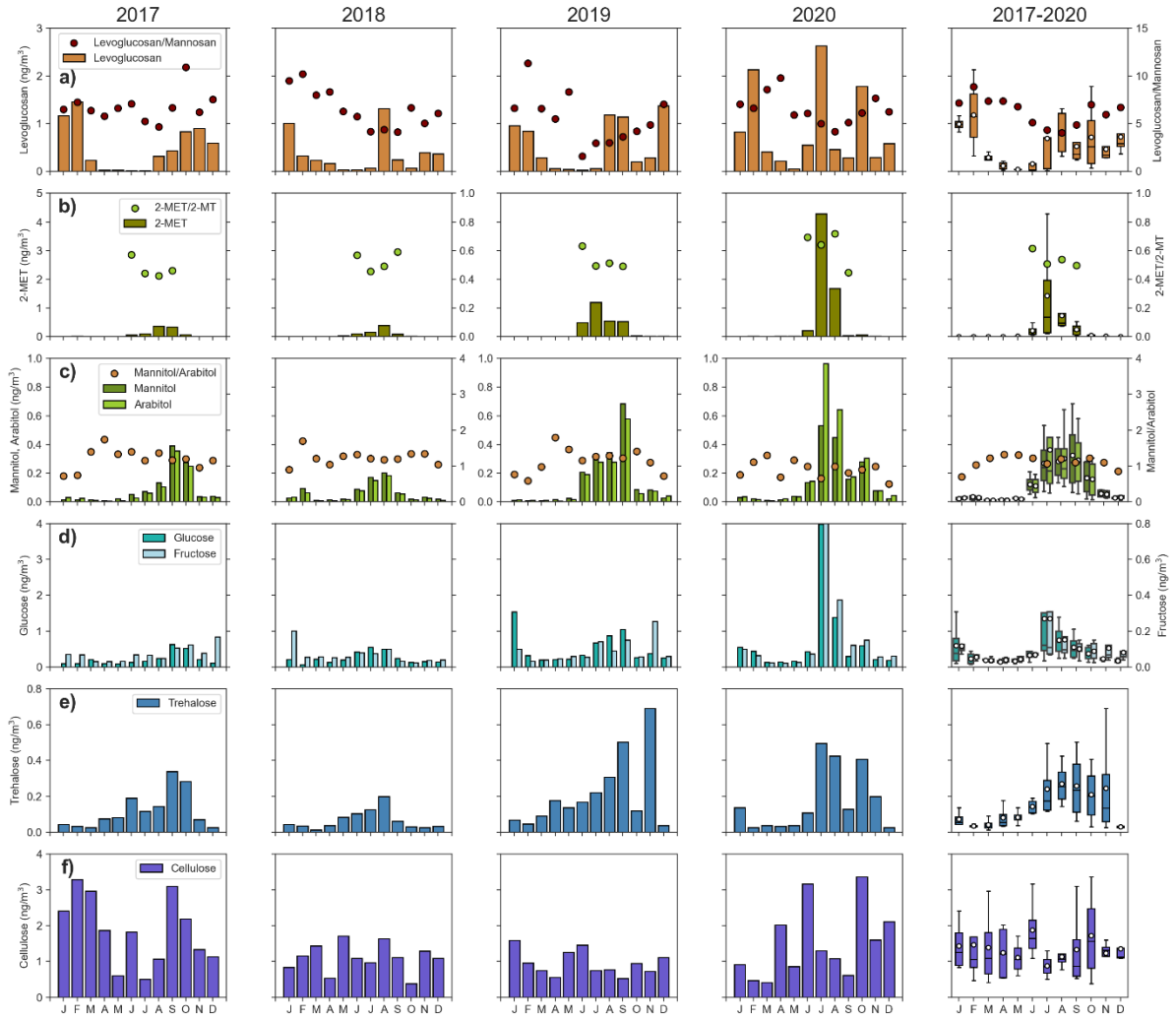

Figure 3. Panels show monthly mean concentrations for 2017 to 2020 and box plots (mean, 25, 50, 75 percentiles and IQR) for 2017 to 2020 at Zeppelin Observatory for a) Levoglucosan and levoglucosan/mannosan; b) 2-methylerythritol (2-MET) and 2-MT/2-MET; c) Mannitol and arabitol and mannitol/arabitol; d) Fructose and glucose; e) Trehalose; f) Cellulose. All variables are measured in the PM_{10} size fraction.

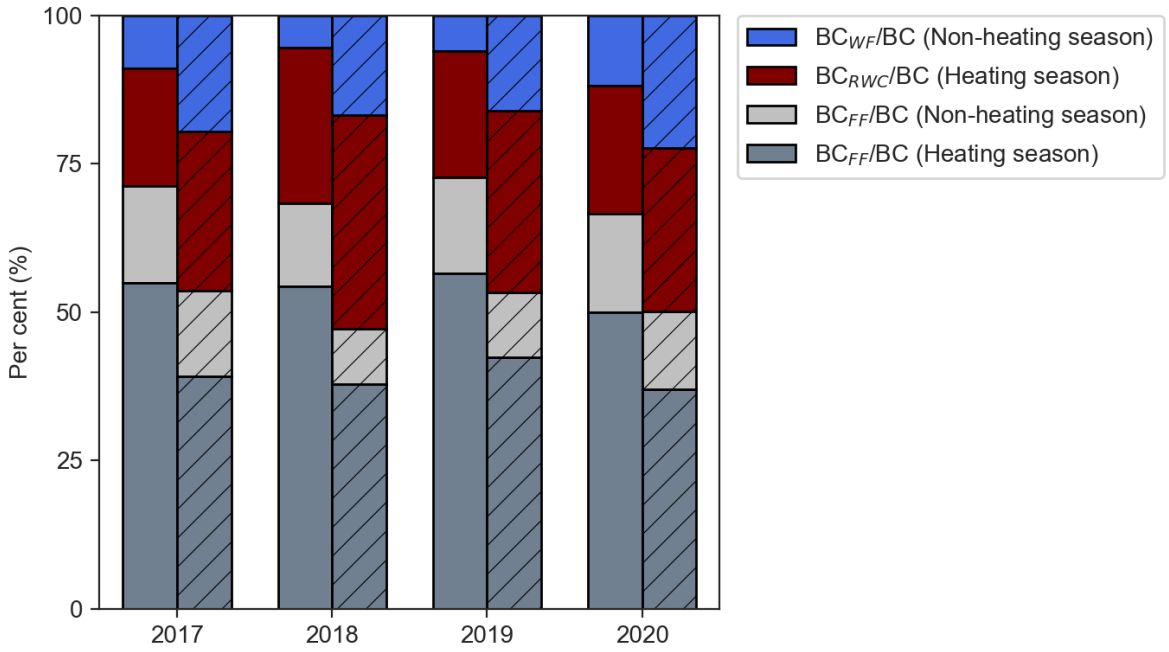

Figure 4. eBC (PMF) (without diagonal lines) and BC (FLEXPART) (with diagonal lines) apportioned to biomass burning (BB) and fossil (FF) fuel combustion according to heating season and non-heating season. BB is denoted wildfire (WF) in summer and residential wood combustion (RWC) in winter. Zeppelin Observatory (2017 to 2020). For simplicity we state BC for all methods, while the correct is eBC for PMF, BC for FLEXPART.

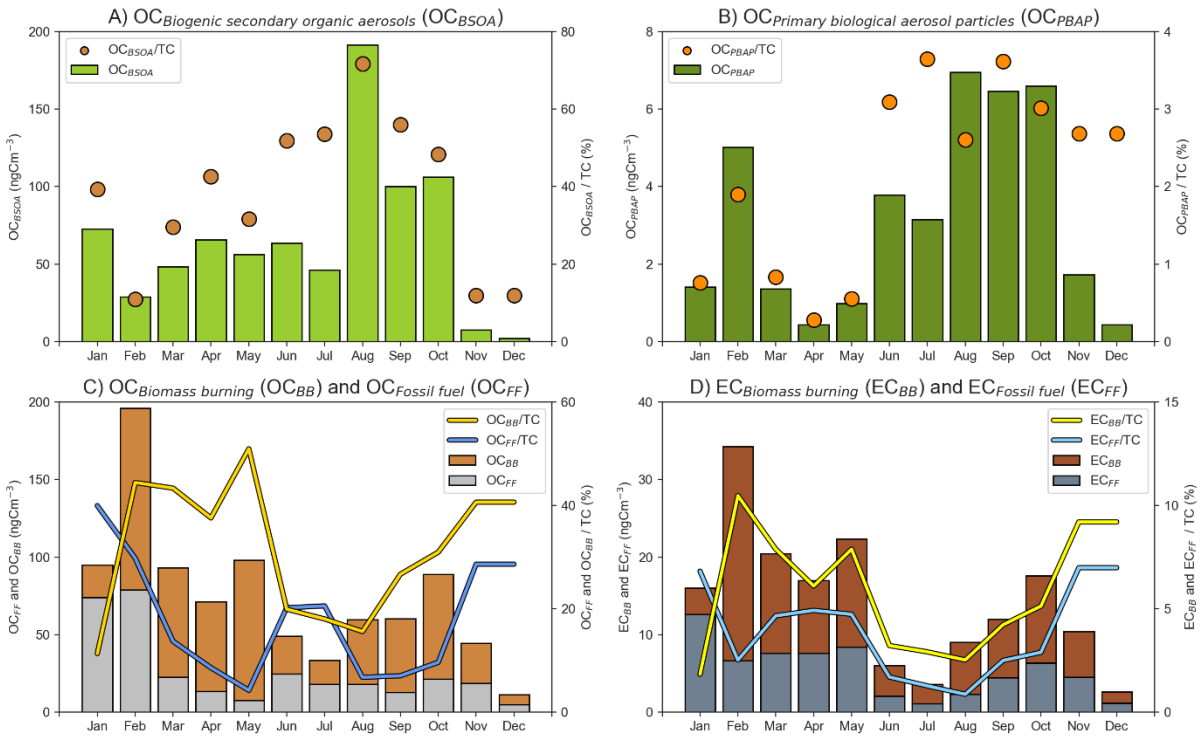

Figure 5. Source apportionment using the LHS approach (Sect. 2.7). Panels show monthly mean concentrations and relative contributions for samples collected in 2017 to 2018 at Zeppelin Observatory for A) Biogenic Secondary Organic Aerosol (OC_{BSOA}) and OC_{BSOA}/TC; B) Primary Biological Aerosol Particles (OC_{PBAP}), being the sum of fungal spores (OC_{PBS}) and plant debris (OC_{PBC}), and OC_{PBAP}/TC; C) Biomass burning (OC_{BB}, OC_{BB}/TC) and fossil fuel sources (OC_{FF}, OC_{FF}/TC; D) Fossil fuel (EC_{FF}, EC_{FF}/TC) and biomass burning (EC_{BB}, EC_{BB}/TC).

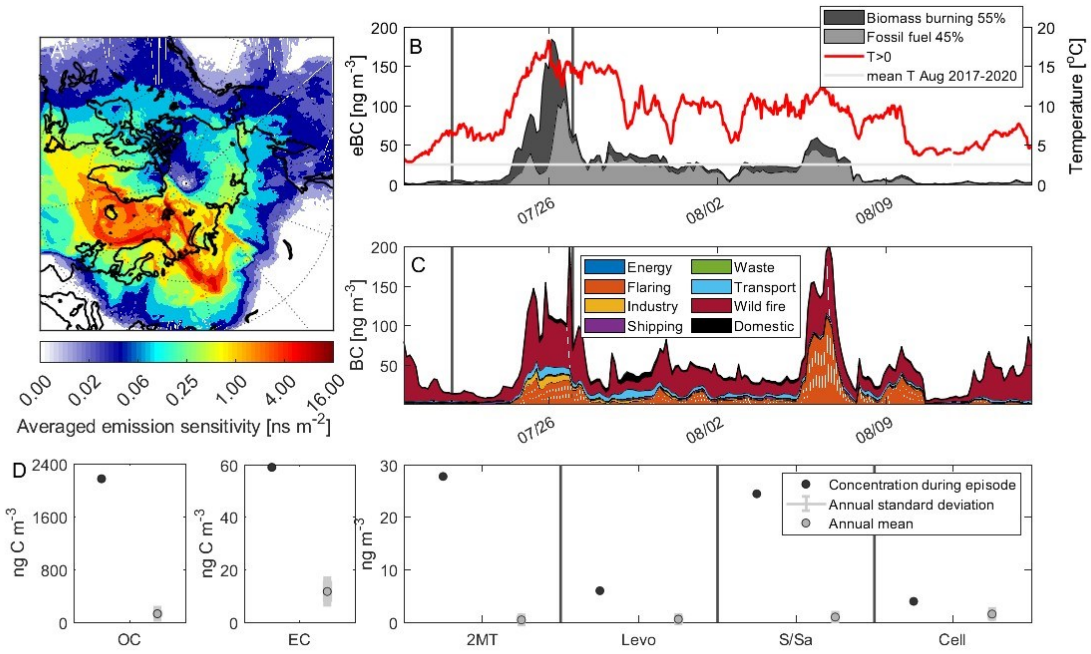

Figure 6. LRT episode at Zeppelin Observatory covered by filter sample collected 22 – 27.07.2020. A) Averaged footprint sensitivity for sample collected 22 – 27.07.2020; B) Hourly time series of eBC_{BB} and eBC_{FF} (PMF) and ambient temperature. The period covered by the filter sample is defined by the dark grey vertical lines; C) Hourly time series of modelled BC concentrations from different source categories; D) Concentrations of OC, EC, and organic tracers (2MT = 2-Methyltetrols; Levo = Levoglucosan; S and SA = Sugars and Sugar-alcohols; Cell = Cellulose) obtained for the filter sample compared to the long-term annual mean and its standard deviation.

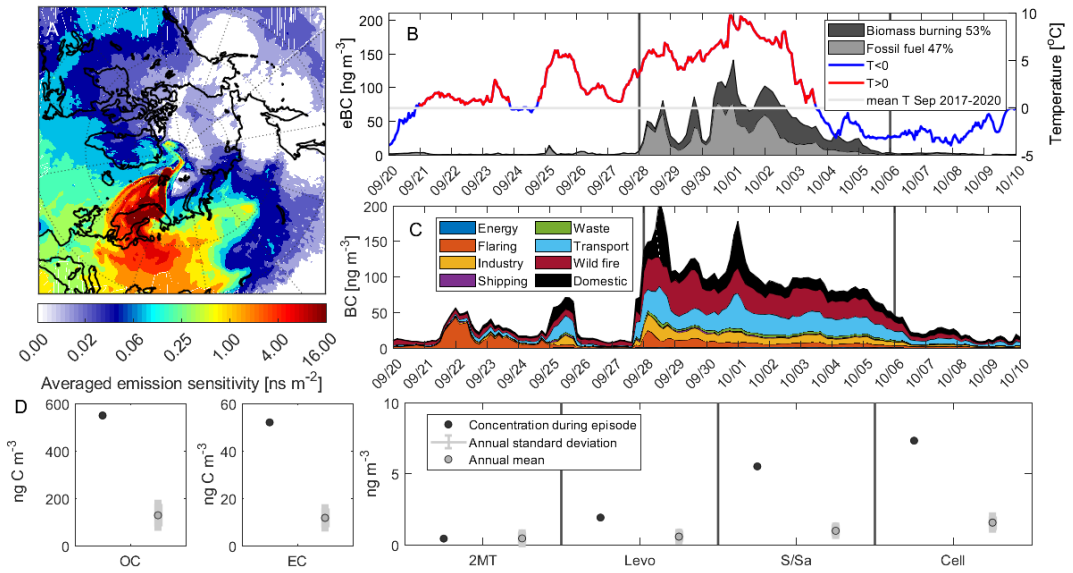

Figure 7. Same as Fig. 6, but for 28.09 – 06.10.2017.

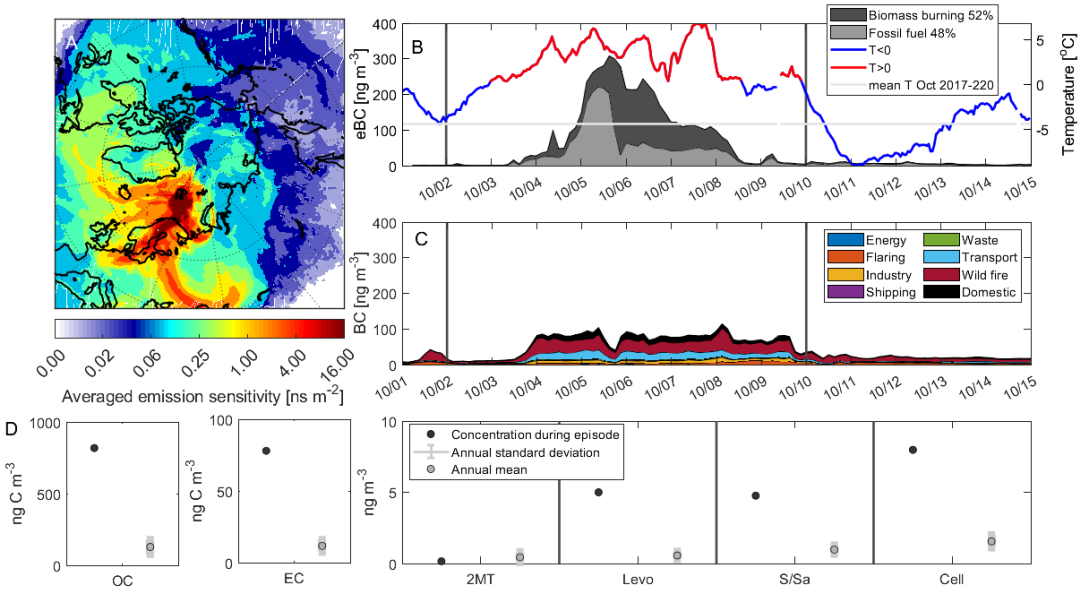

Figure 8. Same as Fig. 6, but for 2 – 10.10.2020.

Supplement of

Composition and sources of carbonaceous aerosol in the European Arctic at Zeppelin Observatory, Svalbard

Table S1: Equations used for source apportionment of carbonaceous aerosol, following the Latin Hypercube Sampling (LHS) approach. See sect. 2.8 and Yttri et al. (2011a) for more details.

$EC = [EC] \times \Phi_{EC}$	(eq.1)
$OC = [OC_p] + \Phi_{NA} \times ([OC_F] - [OC_B])$	(eq.2)
$TC = OC + EC$	(eq.3)
$F_{14C\text{-}TC} = [F_{14C\text{-}TC}] \times \Phi^{14}C\text{-}TC$	(eq.4)
$F_{14C\text{-}EC} = [F_{14C\text{-}EC}] \times \Phi^{14}C\text{-}EC$	(eq.5)
$F_{14C\text{-}OC} = (F_{14C\text{-}TC} - F_{14C\text{-}EC} \times EC/TC) / (1 - EC/TC)$	(eq.6)
$F_{EC\text{-}NF} = F_{14C\text{-}EC} / F_{14C\text{-}BB}$	(eq.7)
$EC_{BB} = F_{EC\text{-}NF} \times EC$	(eq.8)
$OC_{BB} = EC_{BB} \times (OC/EC)_{BB}$	(eq.9)
$EC_{FF} = [EC] - [EC_{BB}]$	(eq.10)
$OC_{PBC} = [Cellulose] \times (OC / Cellulose)_{PBC}$	(eq.11)
$OC_{PBS} = [Mannitol] \times (OC / Mannitol)_{PBS}$	(eq.12)
$OC_{BSOA} = \frac{F_{14C\text{-}OC} \times OC - (F_{14C\text{-}BB} \times OC_{BB} + F_{14C\text{-}PBC} \times OC_{PBC} \times OC_{PBS})}{F^{14}C\text{-}BSOA}$	(eq.13)

Notes:
Square brackets denote measured quantities.
Equation (6) is derived from:

$TC \times F_{14C\text{-}TC} = OC \times F_{14C\text{-}OC} + EC \times F_{14C\text{-}EC}$

$F_{14C\text{-}OC} = (TC \times F_{14C\text{-}TC}\ 1 - EC \times F_{14C\text{-}EC})/OC = (TC \times F_{14C\text{-}TC} - EC \times F_{14C\text{-}EC})/(TC\text{-}EC) = F_{14C\text{-}TC} - EC/TC \times F_{14C\text{-}EC})/(1 - EC/TC)$

Table S2. Emission ratios used for the LHS source apportionment approach of carbonaceous aerosol. Low, central, and high values are listed. See sect. 2.8, Yttri et al. (2011a) for more details.

Parameter	Low	Central	High	Eqn.	Accounts for
Φ_{EC}	0.75	1.0	1.25	1	Uncertainty in EC measurement
Φ_{NA}	0.0	0.2	1.0	2	Negative sampling artefact of OC
$\Phi^{14}C\text{-}TC$	0.95	1.0	1.05	4	Uncertainty in $^{14}C\text{-}TC_{Measurement}$
$\Phi^{14}C\text{-}EC$	0.85	1.0	1.15	5	in $\Phi 14C - EC_{Measurement}$
$\Phi F^{14}C$	1.055	-	1.25	7	Variability in modern carbon age of BB; Notation includes RWC, WF and AWB
$(OC/EC)_{BB}$	3.3	6.2	9.1	9	Wildfires. Derived from Saarikoski et al., (2007); Yttri et al. (2014).
$(OC/Cellulose)_{PBC}$	0.8	1.6	3.2	11	OC_{PBC} calculation
$(OC/Mannitol)_{PBS}$	5.2	-	10.8	12	OC_{PBS} calculation
$F_{14CBSOA}$		1.055		13	Modern carbon
F_{14CPBS}	1.055	-	1.25	13	Fungal Spores
F_{14CPBC}	1.055	-	1.25	13	Plant debris

Table S3: Source apportionment of CA by LHS for samples collected at the Zeppelin Observatory (2017 to 2018). Mean (10th, 50th, 90th percentiles) are provided. Unit: ng C m^{-3}. N/A = Not Available

Start date	End date	OC_{BSOA}	OC_{FF}	OC_{BB}	OC_{PBC}	OC_{PBS}	EC_{FF}	EC_{BB}
23.02.2017	02.03.2017	33 (4.4-27-70)	92 (67-93-115)	137 (107-132-175)	5.7 (3.0-5.1-9.0)	0.1 (0.1-0.1-0.1)	7.7 (3.3-8.0-12)	32 (28-32-37)
05.05.2017	15.05.2017	55 (9.3–49-113)	5.7 (0.8-4.9-12)	97 (63-98-128)	0.7 (0.4-0.6-1.1)	0.0 (0.0-0.0-0.0)	9.0 (6.7-9.0-11)	15 (13-15-17)
31.05.2017	09.06.2017[1)]	64 (37–58-98)	25 (18-24-34)	24 (15-24-34)	3.4 (1.8-3-5.4)	0.41 (0.29-0.41-0.52)	2.1 (1.4-2.1-2.7)	3.9 (3.3-3.9-4.6)
16.06.2017	26.06.2017							
08.09.2017	28.09.2017	52 (27-47-83)	10 (5.7-10-16)	26 (16-25-36)	2.9 (1.6-2.6-4.7)	1.2 (0.84-1.2-1.5)	1.9 (1.2-1.9-2.5)	4.1 (3.5-4.1-4.8)
28.09.2017	06.10.2017	422 (241-384-657)	27 (4.9-24-51)	194 (119-195-266)	13 (7-12-21)	8.9 (6.4-8.9-11)	22 (17-22-26)	30 (26-30-35)
06.10.2017	24.10.2017	18 (3.6-16-37)	20 (13-19-27)	33 (22-31-46)	1.4 (0.7-1.3-2.3)	0.9 (0.6-0.9-1.1)	2.0 (1.1-2.1-2.9)	6 (5.1-5.9-6.9)
05.12.2017	21.12.2017	N/A	N/A	N/A	N/A	N/A	N/A	N/A
23.01.2018	31.01.2018	73 (48-67-106)	74 (56-67-102)	21 (13-21-29)	1.3 (0.7-1.2-2.1)	0.1 (0.1-0.1-0.1)	13 (12-13-13)	3.4 (2.9-3.4-3.9)
21.03.2018	29.03.2018	50 (12-46-94)	14 (5.5-13-23)	62 (39-62-87)	0.7 (0.4-0.6-1.1)	0.1 (0.1-0.1-0.1)	7.6 (5.9-7.6-9.1)	10 (8.9-10-12)
06.04.2018	16.04.2018	66 (24-62-114)	13- (5.1-13-22)	58 (36-57-81)	0.4 (0.2-0.3-0.6)	0.1 (0.0-0.1-0.1)	7.6 (6.1-7.6-9)	9.4 (8-9.4-11)
12.07.2018	30.07.2018	30 (17-27-47)	18 (13-17-24)	13 (7.7-12-18)	1.4 (0.7-1.2-2.2)	1.4 (1.0-1.4-1.7)	1.0 (0.6-1.0-1.3)	2 (1.7-2-2.4)
30.07.2018	15.08.2018	192 (130-174-280)	18 (6.8-17-30)	42 (25-41-59)	4.8 (2.5-4.3-7.7)	2.1 (1.5-2.2-2.7)	2.3 (1.2-2.2-3.3)	6.7 (5.7-6.7-7.8)
23.11.2018	03.12.2018	10 (1.5-7.9-21)	23 (15-24-30)	33 (25-31-42)	1.9 (1-1.7-3.1)	0.2 (0.2-0.2-0.3)	5.6 (4.4-5.7-6.6)	7.4 (6.4-7.3-8.6)

1. Two non-consecutive samples are merged, i.e., 31.05.2023 – 09.06.2023 and 16.06.2023 – 26.06.2023.

Table S4: Source apportionment of CA by LHS for samples collected at the Zeppelin Observatory (2017 to 2018). Mean (10th, 50th, 90th percentiles) percentiles are provided. Unit: %. N/A = Not Available.

Start date	End date	OC_{BSOA}/TC	OC_{FF}/TC	OC_{BB}/TC	OC_{PBC}/TC	OC_{PBS}/TC	EC_{FF}/TC	EC_{BB}/TC	EC_{FF}/EC	EC_{BB}/EC
23.02.2017	02.03.2017	11 (1.7-9.1-21)	30 (25-30-34)	45 (36-45-53)	1.9 (1.0-1.8-2.9)	0.0 (0.0-0.0-0.0)	2.6 (1.0-2.6-4.2)	11 (8.7-10-13)	19 (8.3-20-29)	81 (71-80-92)
05.05.2017	15.05.2017	28 (6-28-52)	3.1 (0.4-2.7-6.6)	54 (34-55-73)	0.4 (0.2-0.3-0.6)	0.0 (0.0-0.0-0.0)	5.1 (3.3-5.1-7.1)	8.5 (6.2-8.5-11)	38 (53-38-72)	62 (28-62-47)
31.05.2017	09.06.2017	51 (37-52-63)	20 (16-20-24)	21 (12-20-31)	2.9 (1.4-2.6-4.8)	0.3 (0.2-0.3-0.5)	1.8 (1.1-1.7-2.5)	3.3 (2.3-3.4-4.3)	34 (24-35-44)	66 (56-65-76)
16.06.2017	26.06.2017									
08.09.2017	28.09.2017	51 (34-53-67)	11 (6.2-11-15)	27 (15-26-41)	3.1 (1.6-2.8-5.2)	1.2 (0.8-1.2-1.7)	2.0 (1.1-1.9-2.9)	4.4 (3.1-4.4-5.7)	31 (20-31-42)	69 (58-69-80)
28.09.2017	06.10.2017	57 (41-58-72)	3.7 (0.7-3.5-7.0)	28 (16-28-42)	1.9 (1.0-1.7-3.7)	1.3 (0.8-1.2-1.8)	3.2 (2.1-3.1-4.3)	4.4 (3.1-4.4-5.6)	42 (33-42-51)	58 (49-58-67)
06.10.2017	24.10.2017	22 (5-21-39)	24 (19-24-29)	41 (27-41-55)	1.8 (0.9-1.7-3.0)	1.1 (0.71-1.1-1.6)	2.6 (1.3-2.6-4.1)	1.9 (1.0-1.7-3.7)	25 (14-26-36)	75 (64-74-86)
05.12.2017	21.12.2017	N/A	N/A	N/A	N/A	N/A	N/A	N/A	N/A	N/A
23.01.2018	31.01.2018	38 (32-39-45)	40 (37-40-43)	12 (7-11-18)	0.7 (0.4-0.7-1.2)	0.0 (0.0-0.0-0.1)	7.1 (5.1-7.4-8.7)	7.6 (5.6-7.5-10)	79 (75-79-82)	21 (18-21-25)
21.03.2018	29.03.2018	33 (9-34-55)	9.3 (4.1-9.3-14)	44 (26-43-64)	0.5 (0.2-0.4-0.8)	0.1 (0.1-0.1-0.1)	5.4 (3.7-5.4-7.3)	7.4 (5.4-7.5-9.5)	42 (33-42-51)	58 (49-58-67)
06.04.2018	16.04.2018	41 (18-43-61)	8.5 (3.5-8.5-13)	39 (22-38-58)	0.2 (0.1-0.2-0.4)	0.0 (0.0-0.0-0.1)	5.1 (3.5-5.1-6.7)	6.3 (4.5-6.38.1)	45 (36-45-53)	55 (47-55-64)
12.07.2018	30.07.2018	44 (31-45-56)	27 (23-27-30)	20 (11-19-30)	2.2 (1.1-1.9-3.6)	2.1 (1.4-2.1-3.0)	1.5 (0.9-1.5-2.2)	3.2 (2.2-3.2-4.1)	32 (21-3.2-42)	68 (58-68-79)
30.07.2018	15.08.2018	71 (60-72-81)	6.8 (2.7-6.7-11)	16 (9-15-24)	1.9 (0.9-1.7-3.2)	0.8 (0.5-0.8-1.2)	0.9 (0.9-1.4-2.0)	2.6 (1.8-2.6-3.4)	25 (13-26-37)	75 (63-74-87)
23.11.2018	03.12.2018	11 (2.1-10-23)	28 (23-28-33)	41 (31-41-49)	2.5 (1.3-2.3-3.8)	0.3 (0.2-0.3-0.4)	7.2 (5.0-7.0-9.9)	9.4 (7.4-9.2-12)	43 (34-44-51)	57 (59-56-66)

Table S5: Annual and seasonal mean concentrations of OC, EC, and organic tracers at Birkenes Observatory (Norway) and at Ispra (Italy), 2017 to 2020.

	OC (μg C m^{-3})	**EC** (μg C m^{-3})	**Levoglucosan** (ng m^{-3})	**Mannosan** (ng m^{-3})	**Galactosan** (ng m^{-3})	**Arabitol** (ng m^{-3})	**Mannitol** (ng m^{-3})	**Glucose** (ng m^{-3})	**Trehalose** (ng m^{-3})	**2-methylerythritol** (ng m^{-3})	**2-methylerythritol** (ng m^{-3})
Birkenes											
2017	**0.72**	**0.05**	**8.24**	**1.35**	**0.32**	**5.52**	**5.70**	**5.17**	**3.37**	**0.37**	**0.10**
DJF	0.57	0.07	15.77	2.49	0.65	1.16	1.40	2.03	1.03	0.01	0.01
MAM	0.65	0.05	7.62	0.98	0.23	3.90	3.65	4.11	1.58	0.05	0.02
JJA	0.92	0.03	2.37	0.48	0.06	9.15	8.45	7.09	4.21	1.32	0.35
SON	0.77	0.06	7.92	1.31	0.29	8.18	9.49	7.58	6.61	0.17	0.06
2018	**0.96**	**0.08**	**9.77**	**1.62**	**0.39**	**5.76**	**5.65**	**4.16**	**2.83**	**0.45**	**0.16**
DJF	0.49	0.07	13.50	2.21	0.60	0.72	0.94	2.74	0.60	0.01	0.01
MAM	1.32	0.11	13.64	2.04	0.54	4.18	4.21	3.59	1.91	0.24	0.08
JJA	1.20	0.05	1.38	0.25	0.04	8.66	7.94	4.52	2.90	1.24	0.42
SON	0.81	0.08	10.64	2.01	0.41	9.38	9.47	5.79	5.91	0.25	0.12
2019	**0.93**	**0.08**	**8.30**	**1.37**	**0.29**						
DJF	0.55	0.09	16.8	2.73	0.61						
MAM	1.44	0.12	8.36	1.20	0.26						
JJA	1.13	0.05	1.32	0.27	0.04						
SON	0.57	0.05	6.91	1.29	0.23						
2020	**0.82**	**0.08**	**7.73**	**1.31**	**0.33**						
DJF	0.31	0.06	7.73	1.29	0.33						
MAM	0.96	0.10	10.7	1.69	0.42						
JJA	1.34	0.06	1.62	0.32	0.04						
SON	0.70	0.09	10.61	1.88	0.50						
Mean ±SD											
Annual	**0.86±0.11**	**0.07±0.01**	**8.51±0.88**	**1.41±0.14**	**0.33±0.04**	**5.64±0.17**	**5.68±0.04**	**4.67±0.71**	**3.10±0.38**	**0.41±0.06**	**0.13±0.04**
DJF	0.48±0.12	0.07±0.01	13.45±4.05	2.18±0.63	0.55±0.15	0.94±0.31	1.17±0.33	2.39±0.50	0.82±0.30	0.01±0.00	0.01±0.00
MAM	1.09±0.36	0.10±0.03	10.08±2.71	1.48±0.48	0.36±0.14	4.04±0.20	3.93±0.40	3.85±0.37	1.75±023	0.15±0.13	0.05±0.04
JJA	1.15±0.18	0.05±0.01	1.67±0.48	0.33±0.10	0.05±0.01	8.91±0.35	8.20±0.36	5.81±1.82	3.56±0.93	1.28±0.06	0.39±0.05
SON	0.71±0.11	0.07±0.02	9.02±1.90	1.62±0.38	0.36±0.12	8.78±0.85	9.48±0.01	6.69±1.27	6.26±0.49	0.21±0.06	0.09±0.04
H-S	0.75±0.18	0.08±0.02	11.90±1.79	1.91±0.30	0.48±0.08	2.50±0.11	2.55±0.14	3.94±0.75	1.39±0.10	0.09±0.04	0.03±0.02
NH-S	1.02±0.09	0.06±0.01	3.70±0.52	0.70±0.09	0.12±0.02	10.11±0.12	10.14±0.46	6.81±1.55	5.56±1.17	0.86±0.04	0.28±0.06
Ispra											
2017	**5.53**	**1.11**									
DJF	10.5	2.19									
MAM	3.37	0.66									

	OC ($\mu g\ C\ m^{-3}$)	**EC** ($\mu g\ C\ m^{-3}$)	**Levoglucosan** ($ng\ m^{-3}$)	**Mannosan** ($ng\ m^{-3}$)	**Galactosan** ($ng\ m^{-3}$)	**Arabitol** ($ng\ m^{-3}$)	**Mannitol** ($ng\ m^{-3}$)	**Glucose** ($ng\ m^{-3}$)	**Trehalose** ($ng\ m^{-3}$)	**2-methylerythritol** ($ng\ m^{-3}$)	**2-methylerythritol** ($ng\ m^{-3}$)
JJA	2.67	0.37									
SON	5.62	1.23									
2018	**3.75**	**0.77**									
DJF	8.30	1.59									
MAM	2.50	0.52									
JJA	1.65	0.31									
SON	2.86	0.73									
2019	**3.82**	**0.80**									
DJF	7.74	1.68									
MAM	2.58	0.57									
JJA	2.46	0.28									
SON	2.40	0.63									
2020	**4.33**	**0.85**									
DJF	7.93	1.74									
MAM	3.06	0.47									
JJA	1.96	0.25									
SON	4.48	0.97									
Mean ±SD											
Annual	4.36±0.82	0.88±0.16									
DJF	8.62±1.28	1.80±0.27									
MAM	2.88±0.41	0.56±0.08									
JJA	2.19±0.46	0.30±0.05									
SON	3.84±1.48	0.89±0.27									
H-S	5.69±0.97	1.19±0.20									
NH-S	2.51±0.64	0.45±0.09									

1. OC, EC, and organic tracers for Birkenes 2017 and 2018 is taken from Yttri et al., (2021), whereas for data for 2019 and 2020 is extracted from ebas.nilu.
2. OC and EC for Ispra is extracted from ebas.nilu

Table S6: Monthly mean ratios of levoglucosan/mannosan, mannitol/arabitol and 2-methylthreitol/2-methylerythritol at Zeppelin Observatory (2017 to 2020) and Birkenes Observatory (2017 to 2018).

	Levoglucosan/ Mannosan		**Mannitol/ Arabitol**		**2-methylthreitol/ 2-methylerythritol**	
Mean (±SD)	Zeppelin Obs.	Birkenes Obs.	Zeppelin Obs.	Birkenes Obs.	Zeppelin Obs.	Birkenes Obs.
January	7.9 ± 1.4	6.5 ± 0.1	0.7 ± 0.2	1.4 ± 0.8	0.72 ± 0.28	0.69 ± 0.00
February	9.0 ± 2.7	6.8 ± 0.6	1.0 ± 0.5	2.3 ± 1.0	0.51 ± 0.06	0.76 ± 0.10
March	7.9 ± 1.2	6.2 ± 0.3	1.2 ± 0.2	1.2 ± 0.2	0.59 ± 0.13	0.76 ± 0.07
April	7.4 ± 3.0	6.6 ± 0.0	1.9 ± 1.2	1.0 ± 0.1	0.61 ± 0.10	0.60 ± 0.00
May	7.2 ± 1.6	7.5 ± 1.0	1.6 ± 0.7	0.9 ± 0.1	0.65 ± 0.09	0.29 ± 0.05
June	5.3 ± 1.2	5.5 ± 0.2	1.3 ± 0.4	1.0 ± 0.2	0.64 ± 0.07	0.29 ± 0.03
July	4.1 ± 0.8	5.7 ± 0.6	1.0 ± 0.3	0.8 ± 0.2	0.54 ± 0.20	0.29 ± 0.28
August	4.2 ± 0.9	4.4 ± 0.2	1.1 ± 0.3	0.9 ± 0.1	0.52 ± 0.13	0.34 ± 0.00
September	5.0 ± 1.7	6.1 ± 1.4	1.1 ± 0.1	1.1 ± 0.2	0.48 ± 0.07	0.42 ± 0.01
October	5.3 ± 1.1	5.4 ± 0.2	1.2 ± 0.3	1.1 ± 0.0	0.54 ± 0.11	0.55 ± 0.10
November	5.7 ± 0.8	5.6 ± 0.5	1.2 ± 0.1	1.0 ± 0.1	0.65 ± 0.17	0.74
December	6.5 ± 1.8	5.4 ± 0.4	1.0 ± 0.5	0.8 ± 0.0	0.74 ± 0.16	0.77 ± 0.09
Annual	**6.0 ± 1.8**	**6.1 ± 0.1**	**1.1 ± 0.5**	**1.0 ± 0.0**	**0.55 ± 0.16**	**0.32 ± 0.05**
DJF	7.8 ± 1.9	6.3 ± 0.7	0.9 ± 0.4	1.5 ± 0.9	0.65 ± 0.13	0.74 ± 0.07
MAM	7.5 ± 2.1	6.7 ± 0.8	1.5 ± 0.8	1.1 ± 0.2	0.62 ± 0.03	0.55 ± 0.22
JJA	4.5 ± 1.2	5.2 ± 0.7	1.1 ±0.3	0.9 ± 0.1	0.56 ± 0.06	0.31± 0.05
SON	5.9 ± 1.1	5.7 ± 0.7	1.1 ± 0.2	1.1 ± 0.1	0.56 ± 0.09	0.54 ± 0.14
NH-S	4.8 ± 1.2	5.4 ± 0.8	1.1 ± 0.3	1.0 ± 0.1	0.54 ± 0.06	0.38 ± 0.11
H-S	7.5 ± 1.9	6.4 ± 0.8	1.2 ± 0.6	1.2 ± 0.6	0.64 ± 0.08	0.65 ± 0.18

Tale S7: Annual mean concentrations of Antarctic baseline aerosol (ABA)[1] OC, EC, and positive artifact corrected OC (OC_P) at Trollhaugen Observatory (Antarctica), 2016 to 2018 and 2021 to 2022. Unit ng C m^{-3}.

	EC	**OC**	**OC_P**
2016	2.0	12.0	7.4
2017	2.3	14.1	10.9
2018	1.4	10.0	7.5
2021	2.0	14.2	9.3
2022	1.7	10.8	7.1
Mean ± SD	**1.9 ± 0.3**	**12.2 ± 1.9**	**8.4 ± 1.6**

Antarctic baseline aerosol (ABA): To differentiate between Antarctic baseline aerosol (ABA) and non-ABA, we relied on input from in-situ on-line nephelometer (TSI 3563) measurements, as defined by Fiebig et al. (2014). We considered values below the 4 weeks running 5th percentile x 2.5 of the aerosol scattering coefficient (σsp, 550 nm) as ABA, while values above this threshold were defined as non-ABA. We made sure not to sample at wind speeds > 10 m s^{-1} to avoid filter damage. We collected ABA and non-ABA using two high-volume samplers (Digitel DHA-80 with a PM_{10} inlet) both with double quartz fibre filters (Pallflex 2500) (McDow and Huntzicker, 1990) to estimate of the positive sampling artifact caused by semi volatile organic compounds (SVOC). The inlet of the nephelometer and high-volume samplers were positioned 5.5 meters above the ground.

Background information to Table S8:

The samples with the highest PBAP and BSOA tracer concentrations were collected in the non-heating Season (June to October). A major fraction of these samples experienced elevated concentrations of the biomass burning tracer levoglucosan, as shown in Table S8. This points to the importance of wildfires for observed concentrations of PBAP and BSOA in the Arctic.

Table S8: Mean concentration of PBAP and BSOA tracers for the top ten highest concentration samples (second column). Mean concentration of PBAP and BSOA tracers for those of the top ten samples collected in the non-heating (NH) season and with a levoglucosan concentration exceeding the long-term mean (third column). Mean concentration of levoglucosan for the samples listed in the third column and their percentiles compared to the long-term mean (fifth column). Zeppelin Observatory, 2017 – 2020.

BSOA and PBAP tracers	**BSOA and PBAP tracers for the top ten highest samples (Mean; Unit ng m^{-3})**	**BSOA and PBAP tracers for those of the topt en samples collected in the NH-season and with $[Levoglucosan]_{Sample} > [Levoglucosan]_{Long\text{-}term\ mean}$ (Mean; Unit: ng m^{-3})**	**BB tracer**	**Levoglucosan for samples listed in column three. Mean (Percentile) (Unit: ng m^{-3})**
Arabitol	1.2	1.3 (n=8)	Levoglucosan	2.7 (96)
Mannitol	1.0	1.1 (n=7)	Levoglucosan	2.4 (95)
Trehalose	1.0	1.0 (n=7)	Levoglucosan	2.4 (95)
Fructose	0.7	1.1 (n=5)	Levoglucosan	3.6 (98)
Glucose	3.5	3.5 (n=9)	Levoglucosan	2.5 (95)
Cellulose	5.7	6.4 (n=3)	Levoglucosan	4.3 (98)
2-Methyltetrols	6.1	7.8 (n=7)	Levoglucosan	2.2 (94)

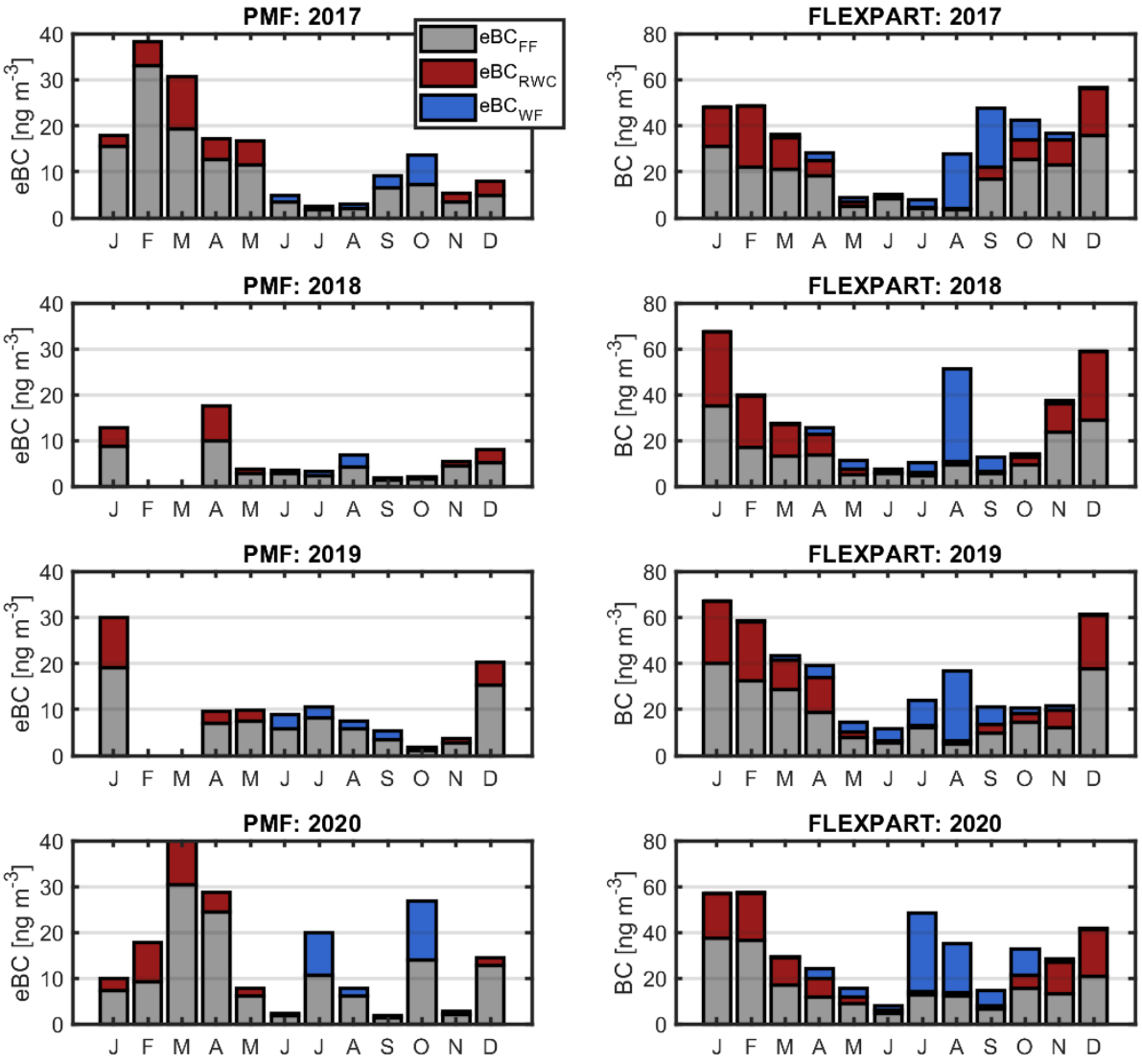

Figure S1. Monthly mean eBC concentrations (PMF) (left) and BC (FLEXPART) (right) apportioned to FF combustion and BB. BB is categorized as RWC in H-Season (red color) and WF in NH-season (blue color). Zeppelin Observatory 2017 to 2020.

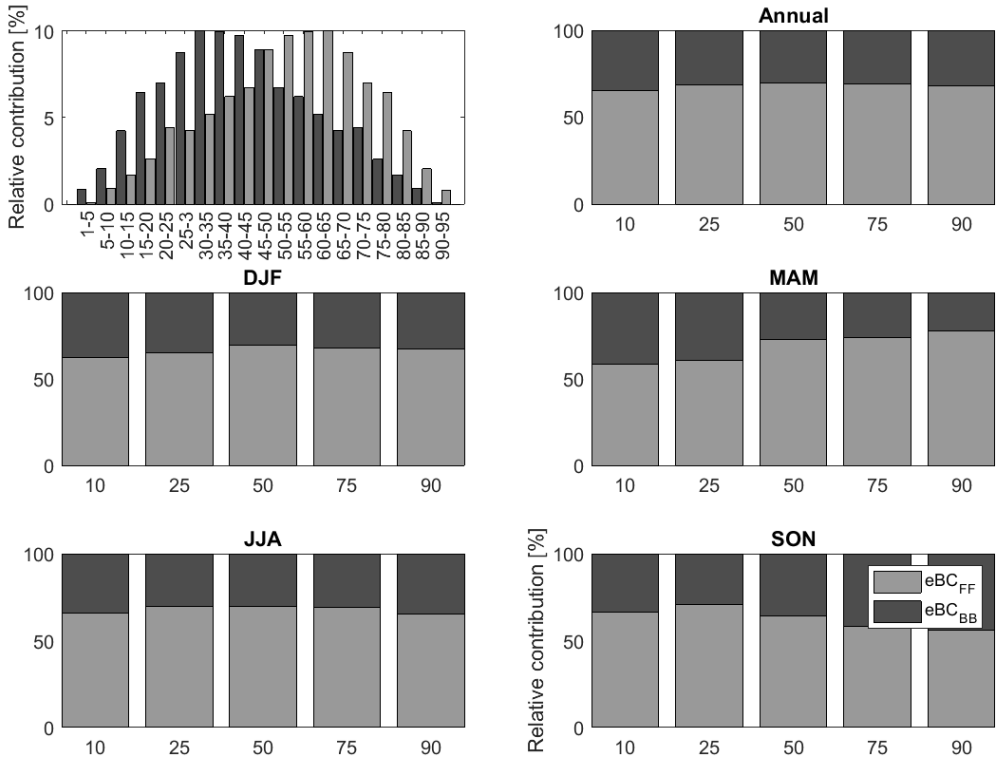

Figure S2. Frequency distribution of eBC_{BB}/eBC and eBC_{FF}/eBC fractions (left top panel), and average eBC_{BB}/eBC and eBC_{FF}/eBC fractions for eBC concentrations below the 10th and the 25th percentile, all observations (50th percentile), and above the 75th and 90th percentiles, for the Zeppelin Observatory, 2017 to 2020. Results obtained by PMF.

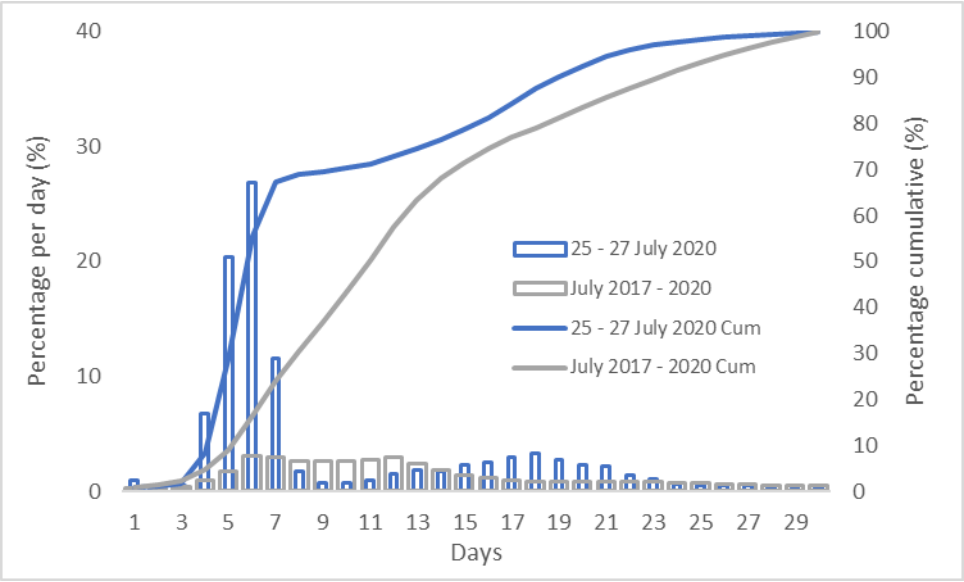

Figure S3. Transport time of modelled BC concentrations from the respective emission sources to Zeppelin Observatory. The blue line are the results for the part of the pollution episode spanning from 25 to 27 July 2020 compared to the reference period (July 2017 to 2020, grey line).